Nuclear orientation of ^{160}Tb in Tb single crystal

H. Marshak
National Bureau of Standards, Gaithersburg, Maryland 20899

W. D. Brewer and P. Roman
Fachbereich Physik, Freie Universität Berlin, Berlin 33, Germany

(Received 26 April 1989)

Nuclear orientation of ^{160}Tb in a Tb single crystal has been carried out in order to obtain accurate values of multipole mixing ratios for 22 transitions in ^{160}Dy. The experimental aspects are described in some detail as they form the basis for obtaining high quality data. Three different methods were used to extract the mixing ratios, and they are shown to agree very well. Our results for both $E1/M2$ and $E2/M1$ transitions are compared to other measurements. The signs and magnitude of the $E1/M2$ mixing ratios cannot be explained on the basis of Coriolis mixing of the $K=0$, 1, and 2 bands. Comparison of our results for the 299, 1178, and 1272 keV transitions with those from γ-γ directional correlation measurements indicate that some $E3$ admixture may be present in these transitions. The mixing ratios we obtained for the $E2/M1$ transitions are in reasonably good agreement with the predictions of the interacting-boson-approximation-1 model.

I. INTRODUCTION

One of the most important requirements for obtaining accurate γ-ray multipole mixing ratios using the low-temperature nuclear orientation (NO) technique is knowing the degree of orientation of the radioactive nuclear spin system. Except for those few cases where the latter can be cooled to a low enough temperature so that only the lowest nuclear spin substrate is populated, accurate values for the hyperfine parameters and the absolute temperature must be known in order to calculate the NO. When possible, the most accurate means of measuring hyperfine parameters for these dilute systems is by nuclear magnetic resonance on oriented nuclei (NMR-ON). Although somewhat difficult, accurate absolute temperature measurements can be made.

The large deformations found in rare-earth nuclei have made this region of the Periodic Table especially important in nuclear physics. For example, measurements of $E2/M1$ multipole mixing ratios in even-even deformed nuclei have played a significant role in testing nuclear models.[1] The rare-earth region has also been very important in solid-state physics. The filling of the electronic $4f$ shell gives rise to very interesting and unusual atomic magnetic properties; e.g., ordering into helical, planar, and linear atomic magnet spin structures.[2] For many of the rare earths, the high orbital angular momentum of the $4f$ electrons also gives rise to very large magnetic fields at the nucleus. In some cases (Ho and Er) the hyperfine fields are over 700 T. These large hyperfine fields enable one to achieve a considerable degree of NO at temperatures which are not too difficult to obtain technically.

Although there have been many nuclear spectroscopy studies of rare-earth nuclei using the NO technique, most of these have been done using samples in which the host material was atomically different. In many cases the host was not even another rare earth. Until very recently[3,4] there were no NMR-ON results for a rare-earth impurity in a rare-earth host, and only three for a rare-earth impurity in a non-rare-earth host.[5-7] Thus, almost all of the nuclear spectroscopic information (multipolarities, moments, and spins) deduced for the rare earths was based on values for the hyperfine parameters which were obtained by less direct means. In many cases the agreement between the NO results and those obtained by other methods was quite good. The largest discrepancies occurred when multipole mixing ratios were compared. As has been pointed out many times, although the directional correlation method has more universal applicability than the NO method, in general it is not able to produce as precise a value for the mixing ratio as the latter. This, of course, stems from the fact that it is a coincidence measurement while the latter is a singles measurement.

With the above in mind, our objective was to do a complete NO study of a rare-earth impurity in a rare-earth host, i.e., the following.

(i) Perform an NMR-ON measurement on the rare-earth system to obtain the hyperfine parameters.

(ii) Do precise absolute temperature measurements in order to calculate accurate values for the NO parameters B_2 and B_4.

(iii) Measure the low-temperature magnetic properties of the system to insure that the magnetic field used in (iv) is sufficient to achieve saturation.

(iv) Finally, make statistically meaningful, γ-ray anisotropy measurements so that accurate mixing ratios can be extracted from the data.

The first consideration of importance in choosing the ideal rare-earth system for this study is that the host material must be a metal single crystal. The reason for this is that the large anisotropy energy associated with the

atomic magnetic ordering precludes magnetic saturation in polycrystalline samples. The host should preferably be monoisotopic so that the radioactivity can be introduced uniformly in the sample by neutron capture. This *in situ* activation leads to substitutional replacement of the host atom without any radiation damage. It should also be possible to prepare samples by ion implantation for the NMR-ON measurements. Finally, the multipole mixing ratios measured should be from a highly deformed even-even nucleus which has previously been studied.

Although the system ^{166}Ho^{m} ($I^{\pi}=7^{-}$) in ^{165}Ho metal single crystal would seem to be the best candidate for this investigation—the properties of the daughter nucleus ^{166}Er (which lies in the middle of the deformed region) have been extensively studied and used on testing nuclear models—it would be very difficult to perform a NMR-ON measurement on this system. Based on the very large hyperfine field in holmium and the large nuclear magnetic moment of ^{166}Ho^{m} ($\sim$4 nm), the resonance frequency is expected to be very high ($\sim$3 GHz). This leads to a very shallow rf-skin depth ($\sim$0.1 μm) for the implanted radioactivity. Also, the nuclear spin-lattice relaxation would be expected to be very fast, making observation of NMR difficult. In addition, the long half-life of ^{166}Ho^{m} (1200 yr) would contaminate the isotope separator used for implantation for an unacceptable time.

The next best candidate for this investigation is the system ^{160}Tb ($I^{\pi}=3^{-}$) in ^{159}Tb metal single crystal. The half-life of ^{160}Tb (72.1 d) is acceptable for ion implantation using an isotope separator. Although the daughter nucleus ^{160}Dy is perhaps not as interesting as ^{166}Er, it too has been well studied. With respect to an NMR-ON measurement, the system ^{160}Tb*Tb*(sc) (sc is the metal single crystal) is much more interesting then ^{166}Ho*Ho*(sc). Most NMR-ON measurements made have been on systems which have a predominant magnetic dipole (Zeeman) hyperfine interaction (hfi). It is known that ^{160}Tb*Tb*(sc), in addition to having a fairly large magnetic dipole hfi ($\sim$1.3 GHz), has a very large electric quadrupole hfi ($\sim$0.2 GHz). The effect of the latter is that there is no longer one resonant frequency (for the magnetic dipole case the $2I+1$ nuclear sublevels are equally spaced), but now $2I$ different subresonance frequencies given by

$$\nu_n=|\nu_M|-\nu_P(2m-1)\ , \tag{1}$$

where ν_M is the magnetic dipole frequency, ν_P is the electric quadrupole frequency, and n is an index numbering the $2I$ frequencies, ν_n given by m going from I to $-(I-1)$. The effect of a positive (negative) quadrupole interaction will result in ν_1 being smallest (largest) for the lowest-energy sublevels; namely, those which have the largest populations at low temperature. Thus, for NMR-ON measurements on rare-earth systems which have large ν_M, a large positive ν_P is helpful in that it lowers the value of the subresonance frequency ν_1. In the case of ^{160}Tb*Tb*(sc), the quadrupole hfi was known to be positive, thus substantially reducing the value for ν_1. The difficulty in NMR-ON measurements on systems which have both dipole and quadrupole hfi is that now one must determine two of the subresonance frequencies (usually ν_1 and ν_2) in order to obtain precise values for both ν_M and ν_P.

We have recently completed NMR-ON measurements on the ^{160}Tb*Tb*(sc) system using both single and double resonance techniques [item (i)].[3,4,8] We have also measured the low-temperature magnetic properties of this system [item (iii)].[9] Since both of these studies have been published (or are to be published) elsewhere, we will only refer here to those points needed in the present work. Here we report on items (ii) and (iv), and on some of the other aspects of our work on the ^{160}Tb*Tb*(sc) system.

II. NUCLEAR ORIENTATION OF ^{160}Tb*Tb*(sc)

The directional distribution of γ rays from an axially symmetric oriented nuclear spin system is given by

$$W(\theta)=\sum_{\lambda} B_\lambda U_\lambda A_\lambda Q_\lambda P_\lambda(\cos\theta)\ , \tag{2}$$

where θ is the angle between the direction of emission of the γ ray and the symmetry axis. B_λ are the nuclear orientation parameters, U_λ are the reorientation coefficients, which correct for the reorientation resulting from the unobserved β and γ transitions preceding the observed γ ray, and A_λ are the directional distribution coefficients, which depend upon the spins of the initial and final states, and the multipole mixing ratio of the γ ray. Q_λ are solid-angle coefficients and $P_\lambda(\cos\theta)$ are Legendre polynomials. Since we are only interested here in the intensity of the directional distribution of the γ rays and not their state of polarization, only even values of λ enter in the summation.

The low-temperature atomic magnetic structure of hexagonal ^{159}Tb single crystals in zero magnetic field is that of a basal plane ferromagnet.[10] The moments lie in magnetic domains in the basal plane along the three b axes of the crystal. These axes are the easy directions of magnetization requiring rather small fields ($\sim$0.5 T in a crystal with a small demagnetization factor) to line up all of the atomic moments (magnetic saturation). Because of the large anisotropy energy, the c axis is the hard direction of magnetization ($\sim$100 T for saturation), whereas the a axes are semihard directions ($\sim$10 T for saturation). Since the hyperfine field is collinear with the atomic moment, it is very advantageous to use a single-crystal sample with the magnetic field along a b axis in an NO measurement. Not only is this beneficial from an experimental point of view, since a small magnetic field can be used to achieve saturation, but it also simplifies the calculation of the NO parameters since, then, there is only one axis of quantization for the entire nuclear spin system.

For a nuclear spin system with axial symmetry, the NO parameters B_λ are

$$B_\lambda=\sum_{m=-I}^{I}(-1)^{I-m}[(2\lambda+1)(2I+1)]^{1/2}\times\begin{bmatrix} I & I & \lambda \\ m & -m & 0\end{bmatrix}a_m\ , \tag{3}$$

where a_m are the populations of the nuclear substrates.

When the nuclear spins are in thermodynamic equilibrium, the populations are given by the Boltzmann factors

$$a_m = \frac{e^{-E_m/kT}}{\sum_m e^{-E_m/kT}}, \tag{4}$$

where E_m are the energies of the nuclear substrates and T is the absolute temperature.

In the case of ^{160}Tb*Tb*(sc), which has both a magnetic dipole and a coaxial electric quadrupole hfi,[8] the energies E_m are

$$E_m = -\left[\frac{\mu\mu_N}{I}B_{\text{eff}}\right]m + \left[\frac{3e^2qQ}{4I(2I-1)}\right][m^2-\tfrac{1}{3}I(I+1)], \tag{5}$$

where the effective field at the nucleus is

$$B_{\text{eff}} = B_{\text{hf}} + (B_{\text{app}} - B_M)(1+K). \tag{6}$$

Since the demagnetizing field B_M can be made fairly small by choosing a favorable sample shape, and as the Knight shift K is quite small ($\sim 1\%$), the applied field B_{app} is only slightly reduced.

The results of our NMR-ON measurements on ^{160}Tb*Tb*(sc) gave (see Table I) $\nu_M = 1386.0(1.2)$ MHz and $\nu_P = 181.2(3)$ MHz.[8] In terms of temperature these values would correspond to hfi splittings of $\Delta_M = 66.517(58)$ mK and $\Delta_P = 8.696(14)$ mK. Since $\nu_M = \mu\mu_N B_{\text{hf}}/Ih$ and $\nu_P = 3e^2qQ/4I(2I+1)h$, B_λ can now be calculated as a function of temperature and for any applied field which is sufficiently large to achieve magnetic saturation.

As mentioned previously, we are only interested in the even values of B_λ (nuclear alignment) here; furthermore, we only have to consider B_2 and B_4 since B_6 plays an insignificant role. Rather than show the temperature dependence of B_2 and B_4, it is more instructive to show their normalized values; i.e., $B_2/B_2(\max)$ and $B_4/B_4(\max)$, where

$$B_\lambda(\max) = (2I+1)^{1/2}\frac{(2I)!}{(2I-\lambda)!}\left[\frac{(2\lambda+1)(2I-\lambda)!}{(2I+\lambda+1)!}\right]^{1/2} \tag{7}$$

These are the values for B_λ when only the lowest-energy nuclear spin substrate is populated.

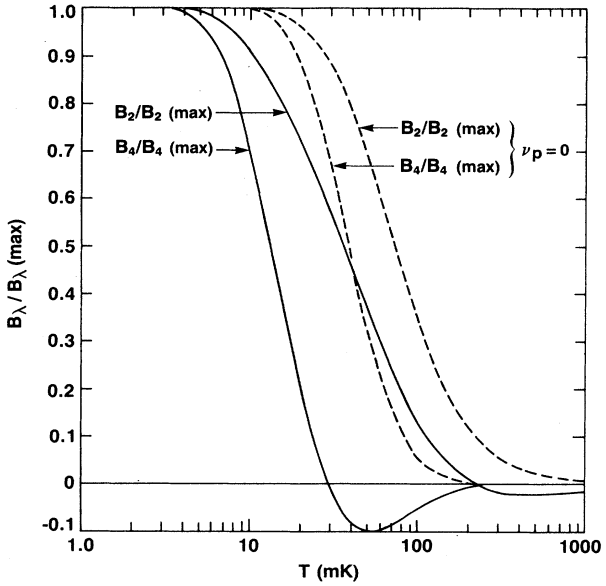

FIG. 1. Normalized nuclear orientation parameters as a function of temperature for ^{160}Tb*Tb*(sc) with and without the quadrupole interaction.

In Fig. 1 we show (solid curves) $B_2/B_2(\max)$ and $B_4/B_4(\max)$ for the case where $B_{\text{app}} = 1.0$ T ($B_{\text{hf}} = 305$ T for Tb). As can be seen, saturation (when essentially only the lowest nuclear substrate is populated) is not achieved until the sample is cooled to ~ 3 mK. In addition, both $B_2/B_2(\max)$ and $B_4/B_4(\max)$ show negative regions. This occurs for any mixed collinear dipole-quadrupole interaction where the latter is positive; i.e., when the energy separation is smallest for the lowest-energy levels, see Eq. (1). For ^{160}Tb*Tb*(sc) it is very pronounced, especially for $B_4/B_4(\max)$, because of the magnitude of the quadrupole interaction. We also show for comparison in Fig. 1 the curves (dashed) for $B_2/B_2(\max)$ and $B_4/B_4(\max)$ for the (fictitious) case where there is no quadrupole interaction ($\nu_P = 0$) in this system. Saturation is now achieved at ~ 10 mK and, of course, neither of these quantities is ever negative. Thus, although the large positive quadrupole interaction helps us in the NMR-ON measurements (by lowering the value for the subresonance frequency), it is a disadvantage for NO, in that we now have to cool to a lower temperature to obtain large values for $B_2/B_2(\max)$, and even so for $B_4/B_4(\max)$. For example,

TABLE I. Hyperfine interaction (hfi) frequencies for ^{160}Tb*Tb*(sc) obtained from NMR on oriented nuclei (Refs. 3, 4, and 8) and from the temperature dependence of the γ-ray anisotropy of oriented nuclei (this work).

	NMR hfi freq. (MHz)		Nuclear orientation freq. (MHz)	
	Annealed sample[a]	Unannealed sample[b]	Global average[c]	Three-parameter fits[c]
ν_M	1384.0±1.7	1386.0±1.2	1393.8±8.1	1388.3±4.5
ν_P	179.7±0.4	181.2±0.3	178.0±2.1	182.4±1.1

[a]Reference 8, sample annealed at 600 °C after implantation.
[b]Reference 4, sample "as implanted."
[c]This work (see text).

at 10, 20, and 30 mK, the values for $B_4/B_4(\max)$ are 0.703, 0.212, and 0, respectively, whereas if $\nu_P=0$ they would be 0.996, 0.885, and 0.673, respectively. This, as we shall see later on, plays a very important role in the analysis for the multipole mixing ratios.

III. EXPERIMENTAL DETAILS

Measurements of the directional distribution of γ rays from oriented ^{160}Tb*Tb*(sc) were made using a ^{3}He-^{4}He dilution refrigerator along with a two-Ge(Li) detector counting system. The unique features of this apparatus are the ability to do accurate low-temperature thermometry and also to maintain very stable temperatures during data acquisition for long periods of time. In addition, either or both detectors can be easily rotated around the sample for detailed studies of the angular dependence of the γ-ray radiation pattern. This feature is very useful in nuclear spin structure studies[11] and also to insure that magnetic saturation is achieved in the sample. A schematic drawing of the lower part of the ^{3}He-^{4}He refrigerator is shown in Fig. 2. The high-purity Tb single-crystal sample used in these measurements was in the form of a rectangular parallelepiped of dimensions $13.5\times3.4\times1.0$ mm^3. The c axis was perpendicular to the flat face and a b axis was along the long dimensions. This sample was spark cut from part of a large disk which was used to produce our NMR-ON samples (see Ref. 8). The flat faces were spark planed and polished to reduce the small amount of surface damage due to spark cutting. X-ray analysis was done to check on the alignment of the crystallographic axes. The uncertainty in the latter was estimated to be about $\pm1°$. The radioactive ^{160}Tb was produced *in situ* in the crystal by activation in the National Bureau of Standards (NBS) reactor. In order to reduce the demagnetizing effects at the ends of the sample, Cd "boots" were used so that only the central 6.5 mm (of the 13.5 mm dimension) were activated. The ^{160}Tb activity was 8.5×10^5 Bq. The sample was attached to an oxygen-free high-conductivity (OFHC) copper mount (using indium solder applied with an ultrasonic soldering iron), which was then screwed into the cold finger of the mixing chamber. From this screw joint, a thick (2.5×12.5 mm^2) OFHC copper thermal link extends to the region within the heat exchanges above the mixing chamber. A six-element superconducting fixed-point device is mounted on the top of this link. Two thin carbon resistance thermometers (T-2 and T-3) are also mounted on this link. A third carbon thermometer (T-1) is mounted below the heater on the cold finger. The superconducting split solenoid can produce a field of 2.0 T.

Accurate low-temperature thermometry is achieved in this apparatus by *in situ* calibration of the carbon thermometers using the six-element superconducting fixed-point device. This device is different from the usual NBS device (SRM-768) (Ref. 12) in that it is miniaturized and contains an extra superconducting fixed point (Cd). The five fixed points (W, Be, Ir, $AuAl_2$, $AuIn_2$) in SRM-768 cover a temperature range of from ~15.5 mK for W to ~204 mK for $AuIn_2$. The inclusion of the Cd fixed point in the present device extends the range to ~520 mK. This extended range is particularly useful in low-temperature experiments where measurements must be made above 204 mK. This device also differs from SRM-768 in that it is magnetically shielded using both Cryoperm and niobium shields. The effectiveness of these shields was measured in fields up to 0.1 T by monitoring the superconducting transition temperature (T_c) of W using a ^{60}Co*Co*(sc) NO thermometer. The results showed no change in the T_c in fields up to 0.05 T, and a very slow change (-0.3 mK/24 h) in a field of 0.1 T. The latter is thought to be due to small impurities in the niobium shield which lower its critical field, normally about 0.2 T. These shields also proved to be very effective in making T_c measurements in the earth's magnetic field (~50 μT) as they are able to attenuate the latter by more than a factor of 500, thus making the use of any compensating coil system unnecessary. The results of these magnetic field studies allow us to conclude that this device can be used in fields of up to 0.05 T (and perhaps slightly higher) without any changes in the T_c of the six fixed points. In our experimental setup (see Fig. 2), this device was mounted 23 cm from the center of the superconducting split solenoid where the fringe field (for a central field of 2.0 T) is <0.01 T.

The T_c's for the six fixed points were assigned by cali-

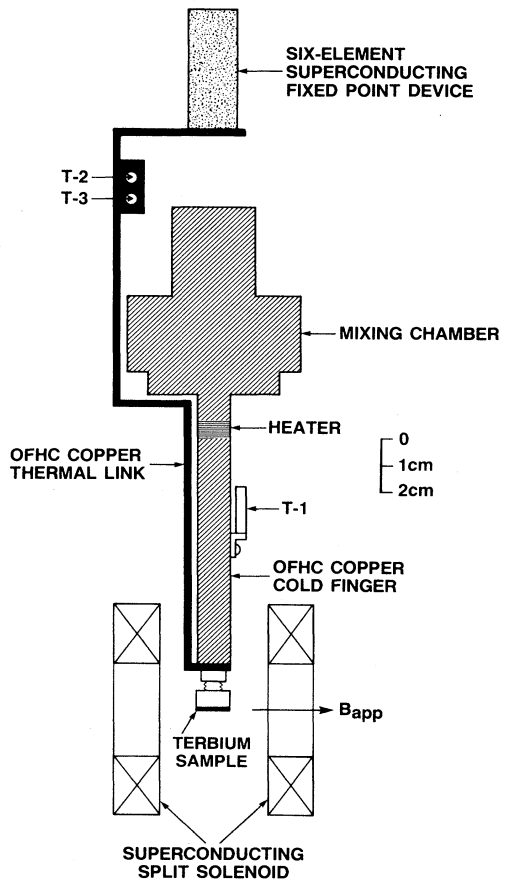

FIG. 2. Schematic drawing of the lower part of the ^{3}He-^{4}He dilution refrigerator.

brating them on the NBS temperature scale CTS-1983 (Ref. 13) which is based on a Josephson junction noise thermometer. The temperatures obtained from the latter are thought to be absolute with an estimated inaccuracy of 0.1%. The temperature assigned to the W-T_c of this device (15.56 mK) by CTS-1983 was independently checked using a ^{60}Co*Co*(cs) NO thermometer. The latter, which should also give absolute temperatures,[14] yielded 15.55 mK for the W-T_c.

We estimate that the method we use here to determine the absolute temperature (*in situ* calibration of carbon thermometers by the six-element superconducting fixed point device along with fifth-order polynomial fits of resistance verses temperature) is inaccurate by no more than ±1%.

Since the ^{160}Tb*Tb*(sc) sample used in these measurements produces about 30 nW of β^- self-heating, a preliminary experiment was performed to insure that there were no temperature gradients between it and the thermal link (as well as the cold finger). It was found that, down to the lowest temperature used in these measurements (18 mK), there was no measurable temperature gradient as long as the indium solder was kept in the normal state. The sample can be held at a constant temperature for periods of days by using one of the resistance thermometers (either *T*-2 or *T*-3) and the cold finger heater in a control feed back loop. Temperature stability to better than 0.1% is achieved in this manner, except near the "bottoming out" temperature of the refrigerator. The latter, which depends upon the heat leak into the mixing chamber, is (for this refrigerator) a strong function of the applied magnetic field due to eddy-current heating. Thus, although the refrigerator can cool to ~12 mK in zero field, it "bottoms out" at 18 mK in 0.5 T and obtains slightly less than 20 mK in 1.0 T. At 1.0 T the temperature stability at 20 mK is only 1%, however, it quickly improves to 0.1% by 25 mK.

The counting system consisted of two ~100 cm^3 Ge(Li) detectors (with 2.0 keV resolution at 1332 keV) connected to a computer-based multichannel analyzer. The output from the amplifier of each detector is recorded in 8192 channels. A temperature stabilized pulser was also connected to both preamplifiers to monitor the live time. The detectors were normally set at 0° and 90°, except when angular dependence measurements were made. For the latter, the 0° detector was always fixed and the second detector rotated. The sample-to-detector distances were purposely kept quite large (27.44 and 30.24 cm, respectively) in order to minimize the solid-angle corrections (as well as their uncertainties). The detectors and the sample were aligned by mechanical means in order to preserve the ±1° uncertainty in the crystallographic axes. $W(0)$, $W(\frac{1}{2}\pi)$, and angular dependence measurements were made by making "warm" and "cold" runs. Since B_2/B_2 (max) goes through zero at ~227 mK (see Fig. 1), and as B_4/B_4(max) is quite small there, it is advantageous to take the warm data in this temperature region rather than to warm up to 4.2 K.[15] All the "warm" runs were made at 223.0 mK, where B_2 is 0.0017 (for $B_{\rm app}=1.0$ T), which is less than its value ($|-0.0067|$) at 4.2 K. A typical run at a fixed temperature consisted of ten one-hour γ-ray spectra. At the completion of each run (while the temperature of the sample was changed and stabilized to a new value, ~0.5 h) the spectra were analyzed using a fairly simple peak-fitting program in order to "keep up" with the data. From these results the mean (counts) and its standard deviation were determined for each peak. These were then used to calculate $W(0)_m \pm \Delta W(0)_m$, $W(\frac{1}{2}\pi)_m \pm \Delta W(\frac{1}{2}\pi)_m$, and $W(\theta)_m \pm \Delta W(\theta)_m$ for the angular dependence data (the subscript m here means "measured"). After the entire experiment was completed, all the spectra (~800) were reanalyzed using the HYPERMET peak-fitting program.[16] In what follows, mainly the HYPERMET results will be used.

IV. DATA ANALYSIS

The explicit form for the angular correlation coefficients A_λ in the case that the γ ray has no more than two multipole orders, namely L and $L'=L+1$, is

$$A_\lambda = \frac{F_\lambda(LLI_2I_1)+2\delta F_\lambda(LL'I_2I_1)+\delta^2 F_\lambda(L'L'I_2I_1)}{1+\delta^2}\ , \tag{8}$$

where the values of the F_λ coefficients are determined by the spins I_1 and I_2 of the initial and final states, respectively, linking the observed γ ray, and its multipole order L. The mixing ratio δ is defined by

$$\delta = \langle I_2 \| L' \| I_1 \rangle / \langle I_2 \| L \| I_1 \rangle\ . \tag{9}$$

There are three methods currently in use for extracting δ values from NO experiments. In the first method, $W(0)_m \pm \Delta W(0)_m$ and/or $W(\frac{1}{2}\pi)_m \pm \Delta W(\frac{1}{2}\pi)_m$ are obtained as function of temperatures, and if B_λ, U_λ, and Q_λ are known, weighted nonlinear least-squares fitting can be done to obtain δ values using

$$W(0,\delta) = 1 + B_2 U_2 A_2 Q_{20} + B_4 U_4 A_4 Q_{40} \tag{10}$$

and

$$W(\tfrac{1}{2}\pi,\delta) = 1 - \tfrac{1}{2} B_2 U_2 A_2 Q_{29} + \tfrac{3}{8} B_4 U_4 A_4 Q_{49} \tag{11}$$

with A_2 and A_4 given by Eq. (8). [Equations (10) and (11) are slightly different from those normally used as they take into account the differences in the Q_λ for the two detectors.] The least-squares fitting, in addition to giving an optimum value for the parameter δ, also gives an uncertainty for δ, $\Delta\delta$, which depends upon the weighted residues of the fit. However, since $\Delta\delta$ does not reflect any uncertainties in the temperature, nor in ν_M, ν_P, U_λ, and Q_λ, it underestimates the "true" uncertainty in δ. In order to take into consideration the uncertainties in B_λ, U_λ, and Q_λ, a Monte Carlo least-squares fitting analysis has to be done. We will designate this first method of obtaining $\delta \pm \Delta\delta$ as the TDLSF (temperature-dependent least-squares-fitting) method.

The second method, which is purely analytical, relies on measurements made at only one temperature (usually the lowest stable temperature available) and solving for δ values using Eq. (8) along with the measured values for A_2 and A_4 (A_{2m} and A_{4m}) found by using

$$A_{2m}=\frac{3[W(0)_m-1]Q_{49}-8[W(\frac{1}{2}\pi)_m-1]Q_{40}}{B_2U_2(3Q_{20}Q_{49}+4Q_{29}Q_{40})} \quad (12)$$

and

$$A_{4m}=\frac{4[W(0)_m-1]Q_{29}+8[W(\frac{1}{2}\pi)_m-1]Q_{20}}{B_4U_4(3Q_{20}Q_{49}+4Q_{29}Q_{40})} . \quad (13)$$

(For most transitions only the A_{2m} equation is used to determine δ.) The uncertainty in δ is found by using first-order propagation of errors to obtain ΔA_{2m} and ΔA_{4m} and using these in Eq. (8). Although the uncertainties in B_λ, U_λ, and Q_λ can be included in ΔA_{2m} and ΔA_{4m}, the resulting $\Delta\delta$ can still be in error.

The third method, which has recently been developed,[17] also relies on measurements made at only one temperature. In contrast to the second method it treats the data using statistical techniques. The mixing ratio (in this case designated $\hat{\delta}$) is obtained using nonlinear least squares, viz.,

$$\mathrm{WSS}(\delta)=\frac{[W(0)_m-W(0,\delta)]^2}{[\Delta W(0)_m]^2}+\frac{[W(\pi/2)_m-W(\frac{1}{2}\pi,\delta)]^2}{[\Delta W(\frac{1}{2}\pi)_m]^2} , \quad (14)$$

where the weighted sum of the squares, WSS(δ), is minimized. Here $W(0,\delta)$ and $W(\pi/2,\delta)$ are given by Eqs. (10), (11), and (8), and using the known values for B_λ, U_λ, and Q_λ. The error in $\hat{\delta}$, $\Delta\hat{\delta}$, is obtained by using noncentral F distribution theory and includes the uncertainties in B_λ, U_λ, and Q_λ. Since this method [subsequently referred to as the Marshak-Spiegelman (MS) method] as well as the second method (subsequently referred to as the A_λ method) have been thoroughly discussed in Ref. 17, we will only touch on the relevant points here. To facilitate presentation of the data we will make use of parametric plots as used in Ref. 17.

V. RESULTS

In the present experiments we were able to analyze data for the 23 γ rays (with $I_\gamma \geq 0.1$ photons/100 decays) shown in the decay scheme in Fig. 3. (The 87 keV γ ray could not be detected because of absorption in the wall of the cryostat.) Of these, 14 are $E1$ with possible small admixtures of $M2$, four are $E2/M1$, one is pure $E2$ and three are $E2$ with possible small admixtures of $M3$. One of the $E1/M2$ transitions (1178 keV) is thought[18] to also have some $E3$ admixture. In addition, the 4^- spin assignment for 1386 keV level has been questioned;[19] in-

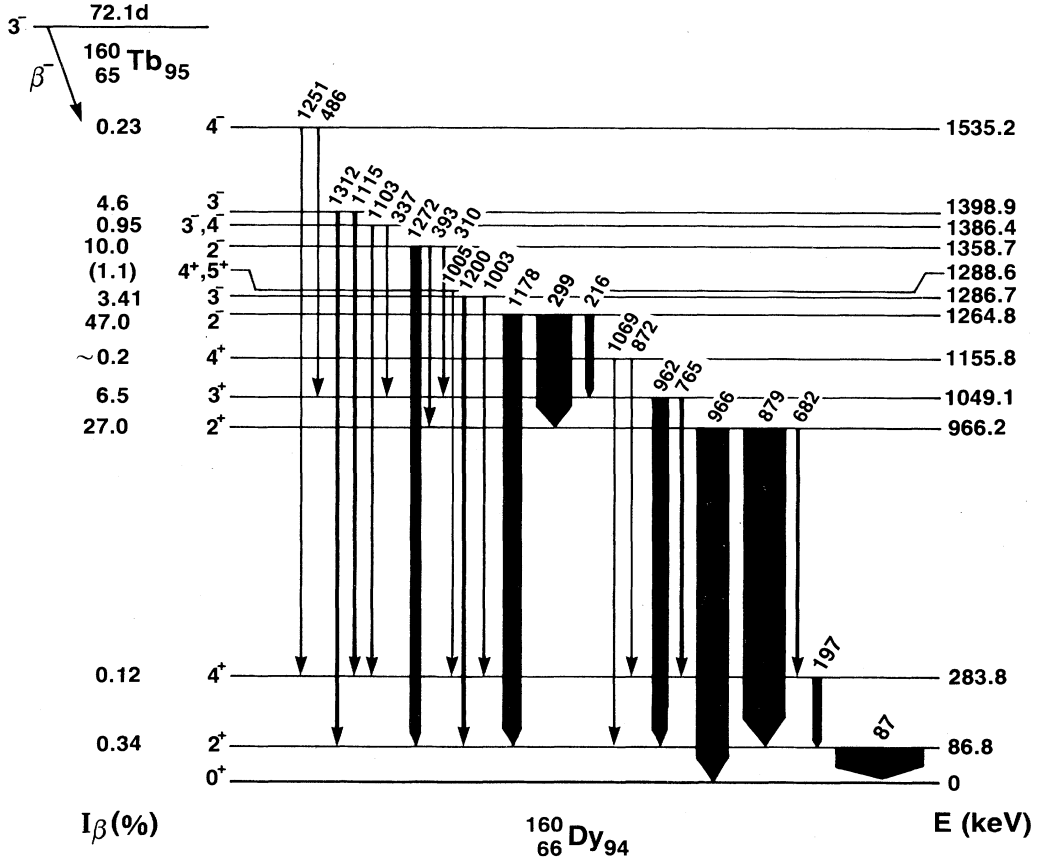

FIG. 3. Decay scheme of ^{160}Tb to ^{160}Dy. Only the transitions measured in the present experiment (with the exception of the 87 keV transition) are shown.

stead, it may be 3^-. In Table II we give the values used for U_2 and U_4 for all the levels shown in Fig. 3, with the exception of the 87 keV level. These were calculated using the I_β values and branching ratios given in Lederer and Shirley,[20] and assuming only $L=1$ for all the β^- transitions. For some of the latter a small $L=2$ contribution is possible. This point, along with the uncertainties in the U_λ, is discussed later when the results for the individual γ rays are presented. The values for the Q_λ for each γ ray were calculated using the method of Krane.[21] These range from $Q_{20}=0.9942$ and $Q_{40}=0.9806$ at 197 keV to $Q_{20}=0.9946$ and $Q_{40}=0.9821$ at 1312 keV, with the values for the second detector (usually at $\frac{1}{2}\pi$) being slightly higher. The uncertainties in the Q_λ were estimated by imposing significant variations in all the parameters entering into the calculation and resulted in $\Delta Q_{20}=\pm 0.05\%$ and $\Delta Q_{40}=\pm 0.2\%$, and similar values for the second detector.

Since the bulk ^{160}Tb*Tb*(sc) sample used in these measurements was prepared differently from the implanted ^{160}Tb*Tb*(sc) sample that we used in our NMR-ON experiments, we first had to establish the hfi parameters obtained for the latter can also be used for a bulk sample. However, before we could do this we had to determine the field strength needed to achieve magnetic saturation in our bulk sample (see Sec. II). This was done by first making a series of "cold" ($T=25.0$ mK) and "warm" runs to obtain $W(0)_m$ as a function $B_{\rm app}$ from 0 to 1.15 T. The results for the intense ($I_\gamma=29.4$) 299 keV transition are shown in Fig. 4(a). In addition to the five data points shown [the errors $\Delta W(0)_m$ are all smaller than the size of the circles] we show calculated saturated values for $\delta=0$ (dashed line) and $\delta=0.02$ (solid line). As can be seen, the latter value (which is close to the value we measure for this transition) agrees quite well with the data. The measured value (0.9254 ± 0.0023) for $B_{\rm app}=0$ also agrees fairly well with the calculated value (0.9159), for which $\frac{1}{3}$ of the atomic moments lie along each of the b axes (0° and ±60°), see Sec. II. (Closure domains and Bloch walls were not taken into consideration in the calculated value and will change it slightly.) Although magnetic saturation seems to be achieved at 0.5 T for this sample, we decided to use 1.0 T for most of our measurements. As a further check that the sample was magnetically saturated (at 1.0 T), angular dependence measurements were made. Since B_4 is quite small (0.0522) at 25.0 mK, and as A_4 for the 299 keV γ ray depends only upon δ^2 and thus is also quite small (using $\delta=0.02$), the angular dependence for this transition is essentially given by $P_2(\cos\theta)$. In Fig. 4(b) we show $W(\theta)$ measurements for this γ ray in the region around the "magic angle," for which $P_2(\cos\theta)=0$; i.e., $\theta=54.75°$. We also show the calculated angular dependence at saturation for the same two δ values that were used in Fig. 4(a). Although the data points have larger errors than those in Fig. 4(a) (the counting time used was a factor of 4 shorter in these measurements), $\delta=0.02$ is still favored. At $\theta=54.75°$ the value for $W(\theta)_m\pm\Delta W(\theta)_m$ (1.0051 ± 0.0054) is in good agreement with the calculated value (1.0001). However, even better agreement can be obtained for it, as well as the four other data points, if we assume an angular error of $+0.5°$ between the angular detector and a b axis ($+60°$). This $+0.5°$ shift in the $\delta=0.02$ curve is shown by the dot-dashed curve in Fig. 4(b) and, as can be seen,

TABLE II. Reorientation coefficients U_λ. These were calculated assuming $L=1$ for all the β^- feeding.

Energy level (keV)	U_2	U_4
283.8	0.563 37	0.065 87
966.2	0.613 08	0.056 45
1049.1	0.719 96	0.191 09
1155.8	0.902 30	0.673 46
1264.8	0.826 90	0.417 51
1286.7	0.750 00	0.166 67
1358.7	0.828 08	0.417 86
1386.4	0.904 68	0.681 38
1398.9	0.750 00	0.166 67
1535.2	0.904 68	0.681 38

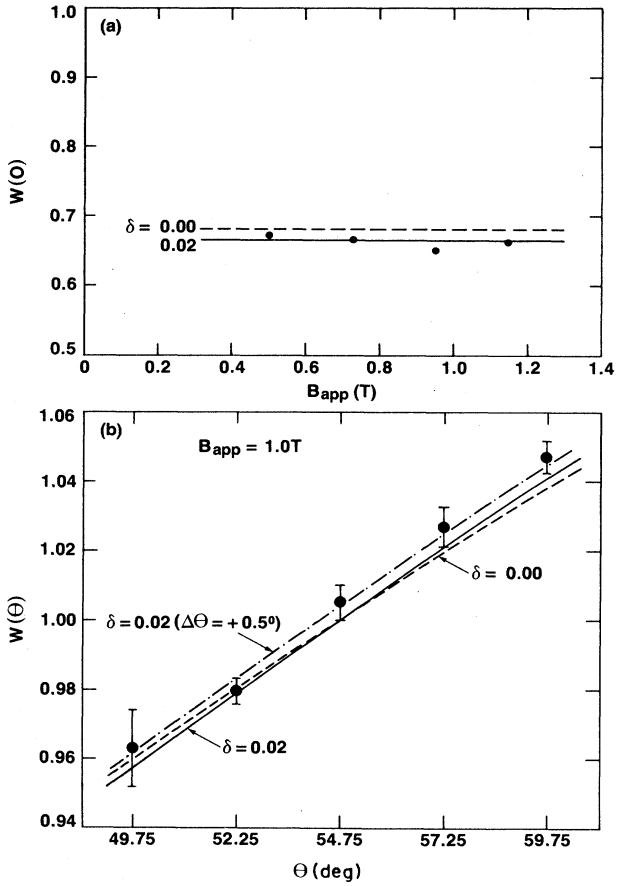

FIG. 4. Magnetic saturation of the Tb*Tb*(sc) sample used in the present experiment; (a) $W(0)$ vs the applied field for the 299 keV transition, (b) $W(\theta)$ vs θ for the same transition in the region around $P_2(\cos\theta)=0$. Fits are shown for two δ values.

the agreement is now excellent. Some idea of the sensitivity of this method can be obtained if we use a magnetization model in which the atomic spins lie only along the b axes.[9] In this case, magnetizations of 0.99 and 0.98 would give calculated values for $W(54.75°)$ of 0.9932 and 0.9864, respectively. Thus, we can conclude that our sample is magnetically saturated at 1.0 T, with perhaps an error of $+0.5°$ in our detector alignment.

In order to determine the hfi parameters for the bulk sample, and also to deduce mixing ratios, values for $W(0)_m \pm \Delta W(0)_m$ and $W(\frac{1}{2}\pi)_m \pm \Delta W(\frac{1}{2}\pi)_m$ were obtained as a function of temperature from 20 to 150 mK with $B_{\rm app}=1.0$ T. With the exception of a run at 20.88 mK, runs were made every 5 to 50 mK, then every 10 to 100 mK and then every 25 to 150 mK. Since the A_λ and MS methods of deducing mixing ratios depend upon measurements made at only one temperature (see Sec. IV), repeat runs were attempted at 20 mK to improve the statistical precision of the data. However, because of the difficulty in temperature stabilization (at $B_{\rm app}=1.0$ T, see Sec. III) repeat runs (3) were made at 25 mK. In addition, two runs were made with $B_{\rm app}=0.5$ T at 18.07 and 25 mK.

A. Multipole mixing ratios using the TDLSF method and LSF for hyperfine parameters

We discuss separately the three different methods used to derive multipole mixing ratios for the γ rays of ^{160}Dy. The TDLSF method has the advantage of making use of all the temperature data in a single fit (the measured anisotropies at 0° and 90° were, in general, fitted separately and the results combined as weighted averages, although combined fits could be and were carried out in some cases, also). Furthermore, it allows the simultaneous determination of the hyperfine parameters by means of a multiple-parameter fit; i.e., by allowing ν_M and ν_P, as well as δ to be free parameters.[22] However, as pointed out earlier, precise estimation of the experimental errors is difficult, since both the anisotropies and the temperature are subject to uncertainties, as are the U_λ and Q_λ coefficients. In general, the "fit errors" calculated by the LSF program seriously underestimate the true experimental uncertainties, since they do not include errors in the temperature scale and in the coefficients. Some idea of the true uncertainties could be obtained by systematically varying the coefficients (and the temperature scale), but this procedure is approximate at best. Thus, two types of LSF analysis were undertaken: three-parameter fits, in which δ, ν_M and ν_P were varied simultaneously; and single-parameter fits, in which the hyperfine parameters were held fixed at the NMR values and only the δ value was allowed to vary [in some cases the ratio R of $(L=2)/(L=1)$ components in a preceding β decay was also allowed to vary]. Figure 5 summarizes the fit results for six of the predominantly $E1$ γ rays. The $W(0)_m$ and $W(\frac{1}{2}\pi)_m$ data are shown as points with their statistical errors $\Delta W(0)_m$ and $\Delta W(\frac{1}{2}\pi)_m$. The solid curves are the results of three-parameter fits, and the dashed curves are from single-parameter fits using the unannealed NMR results for ν_M and ν_P. The agreement, as can be seen, is excellent, especially for stronger γ rays which have small statistical uncertainties (note that the 299, 1178, and 1272 keV transitions are fairly intense, having relative intensities $I_\gamma=29.4$, 16.2, and 8.1%, respectively, while the 1200 keV transition has $I_\gamma=2.58\%$, the 393 keV 1.4%, and the 337 keV only about 0.4%). We emphasize that the hyperfine parameters obtained in this manner represent a completely independent determination from that of our NMR experiments. Here we measure the hyperfine splitting energies by comparison to an absolute temperature scale, while the NMR results are obtained from a comparison to the frequency of an applied rf field. The associated systematic errors are quite different in the two cases. Furthermore, the samples used in the present measurements and in the NMR experiments were prepared in very different ways, as described above. For an accurate determination of the hyperfine parameters from the temperature dependence of the NO, it is necessary to have access to an absolute temperature scale over a wide range of temperatures, and to perform precise anisotropy measurements over as much of this range as possible. This is particularly important in the case of a mixed magnetic dipole-electric quadrupole hyperfine interaction, as can be seen in Fig. 1: the main effect of the quadrupole interaction is to shift the orientation parameters along the temperature axis, and, in particular, to change the location of the "knees" in the anisotropy curve, where the approach to a constant (saturation) value at low temperatures and to the isotropic value at high temperatures occurs. In fact, the low-temperature knee is between roughly 5 and 15 mK for ^{160}TbTb(sc) (Fig. 1), and the B_4 term in Eq. (2) is significant only below about 15 mK; it would thus have been desirable to carry out the present measurements to at least 10 mK, since the B_4 term can be important in deciding between different possible solutions for δ (see below). Nevertheless, the excellent accuracy and reproducibility of our temperature scale over the range of 15–500 mK and the precise anisotropy data obtained between 18 and 150 mK allows us to determine accurately the hyperfine parameters for this system by fitting the temperature dependence, as we shall demonstrate.

In some cases, the three-parameter fits behaved badly, tending to extreme (and unphysical) values of one of the parameters or depending strongly on the starting values used, indicating the presence of secondary minima in the parameter space. In such cases, we performed two-parameter fits, in which one hyperfine frequency was held constant at the NMR value, while the other frequency and δ were allowed to vary; the roles of the hyperfine frequencies were then reversed and the procedure repeated. The weighted averages for ν_M and ν_P are given in Table I along with the NMR results. It may be seen that the agreement is excellent; furthermore, the average frequencies from the three-parameter fits alone agree well with the global averages from all γ rays for both two- and three-parameter fits, indicating that the former do not prejudice the fitted value of the hyperfine frequency. This consistency verified that the hyperfine parameters are insensitive to the different sample preparation techniques, and that the NMR values may be applied to the present data from bulk samples. It also demonstrates the feasibil-

ity of obtaining hyperfine parameters from NO data, to an accuracy of better than 0.6% for the magnetic interaction frequency and 1.2% for the quadrupole interaction frequency in the present case. This is an important demonstration for future applications, particularly in cases where NMR on radioactive isotopes is difficult or impossible, e.g., in on-line implantation facilities.

In the remaining discussion of the analysis for the mixing ratios, we use the more precise (unannealed sample) NMR values of the hyperfine parameters, which have now been shown to be applicable to the bulk sample used in this work.

The problem of determining the multipole mixing ratios is somewhat different in the cases of the predominantly $E1$ and the predominantly $E2$ transitions. The $M2/E1$ transitions are all preceded by allowed beta decays, most of which have pure Gamow-Teller ($L=1$) character; thus the corresponding $U_\lambda(\beta)$ coefficients are exactly known. Exceptions are the decays to the 3^- levels at 1286.7 and 1398.6 keV, which could contain Fermi ($L=0$) admixtures. The resulting uncertainties in the δ values for the 1003, 1115, 1200, and 1312 keV γ rays will be discussed below. The δ values for these $M2/E1$ transitions are rather small, and in many cases, previous

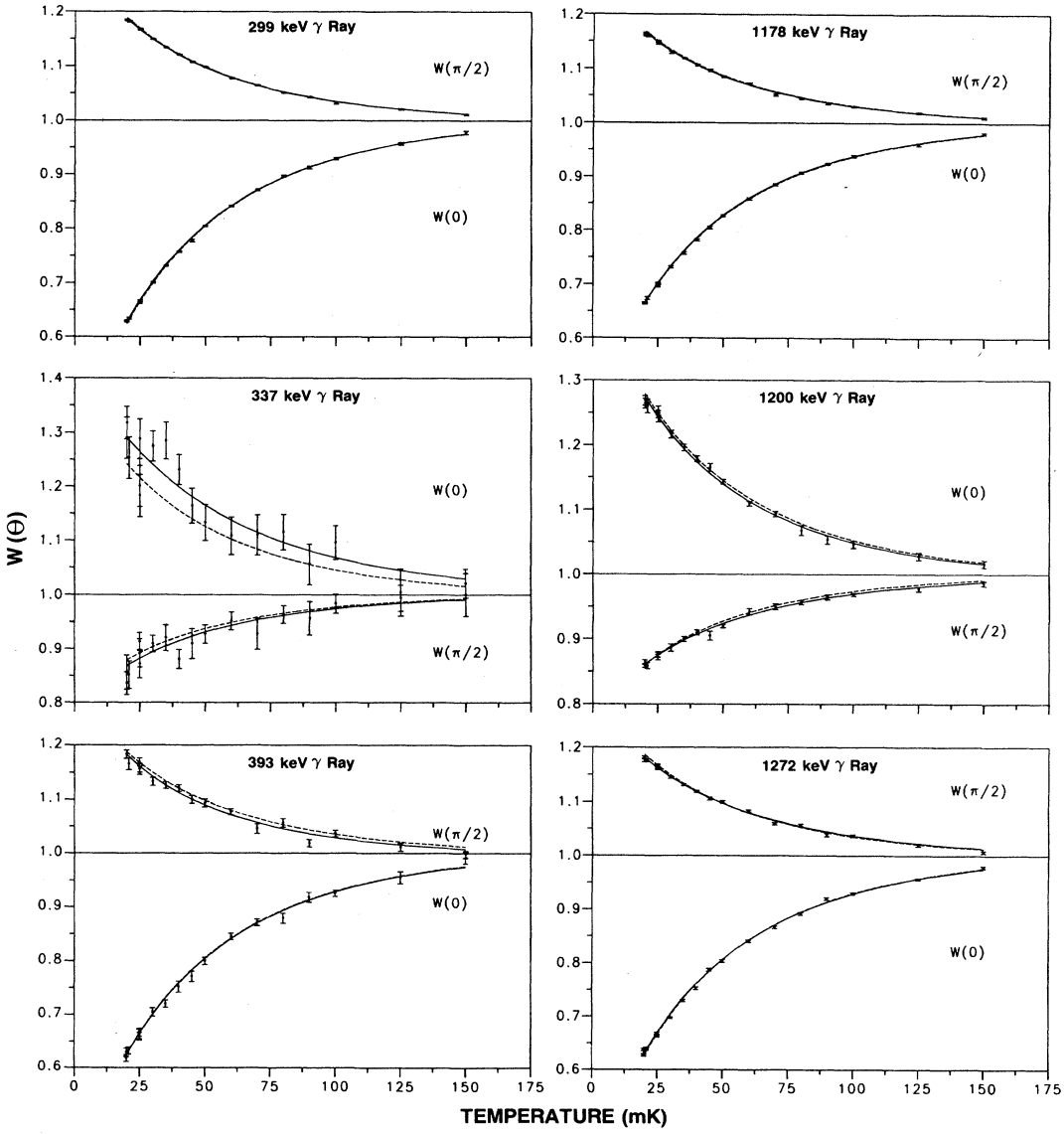

FIG. 5. $W(0)$ and $W(\frac{1}{2}\pi)$ as a function of temperature for six $M2/E1$ transitions. The solid and dashed curves are weighted least-squares fits to the data (see text).

determinations have shown them to be consistent with vanishing $M2$ admixtures. Our results for δ of the 14 $M2/E1$ transitions by the TDLSF method are given in the first column of Table III.

The predominantly $E2$ transitions, by contrast, are fed not only by preceding $E1$ γ rays, but also directly by first-forbidden β decays, all of which could, in principle, contain an $L=2$ admixture to the dominant $L=1$ character. (In one case, the decay to the 3^+ level at 1049 keV, an $L=0$ admixture is also possible.) Three of these transitions (at 197, 682, and 1069 keV) are of $M3/E2$ multipole character, with vanishing $M3$ admixtures. One of them, the 966 keV transition, is pure $E2$ and is thus a key transition for unraveling the entire decay scheme. The remaining four γ rays treated in this work, at 765, 972, 879, and 962 keV, are of $E2/M1$ character, with relatively large $M1$ admixtures of several percent or more. Figure 6 shows the data and corresponding fits for four of these predominantly $E2$ transitions, two of $M3/E2$ and

TABLE III. $M2/E1$ multipole mixing ratio results for ^{160}Dy using the TDLSF, A_2, and MS methods.

E_γ (keV)	$\delta\pm\Delta\delta$	$\delta_2\pm\Delta\delta_2$	$\hat{\delta}\pm\Delta\hat{\delta}$
216	+0.0006±0.0021	+0.0087±0.0046	+0.0046±0.0053
299	+0.0168±0.0004	+0.0188±0.0023	+0.0188±0.0024
310	−0.0108±0.0320	−0.0073±0.0063	−0.0134±0.0072
337	+0.0024±0.0053	+0.0306±0.0108	+0.0284±0.0128
393	+0.0169±0.0021	+0.0131±0.0067	+0.0181±0.0057
486	+0.0670±0.0742	−0.0134±0.0391	+0.0357±0.0287
1003	+0.0044±0.0023	+0.0044±0.0056	+0.0010±0.0049
1103	+0.0056±0.0043	−0.0082±0.0131	+0.0049±0.0121
1115	−0.0006±0.0016	−0.0004±0.0034	+0.0012±0.0032
1178	−0.0212±0.0005	−0.0210±0.0022	−0.0207±0.0023
1200	−0.0063±0.0011	−0.0077±0.0026	−0.0077±0.0029
1251	−0.0023±0.0146	−0.0024±0.0335	−0.0058±0.0312
1272	+0.0147±0.0006	+0.0137±0.0031	+0.0166±0.0025
1312	−0.0139±0.0010	−0.0147±0.0025	−0.0149±0.0028

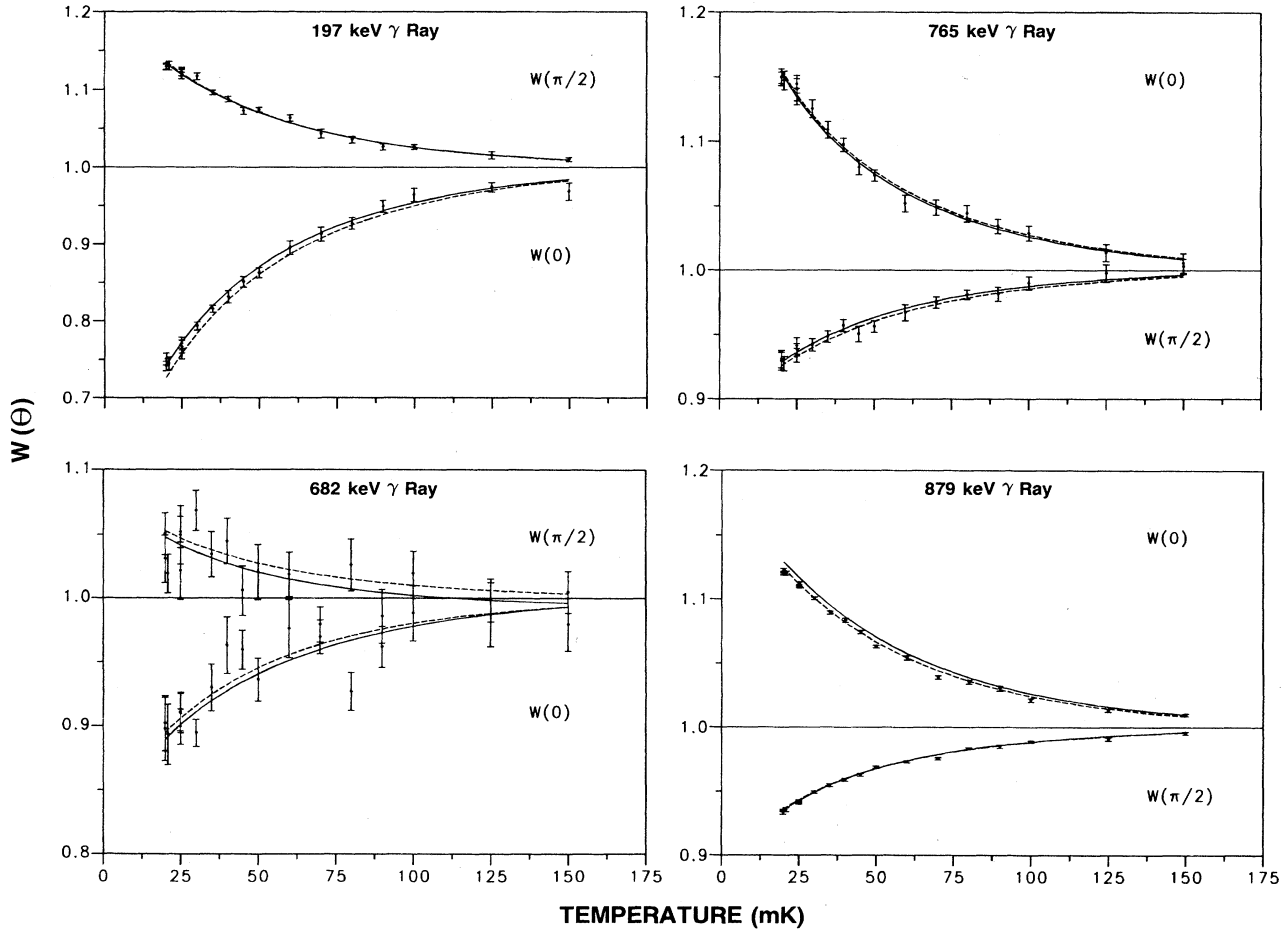

FIG. 6. $W(0)$ and $W(\frac{1}{2}\pi)$ as a function of temperature for two $M3/E2$ (197 and 682 keV) and two $E2/M1$ (765 and 879 keV) transitions. The solid and dashed curves are weighted least-squares fits to the data (see text).

two of $E2/M1$ character. The results for the four $E2/M1$ transitions are given in Table IV, and those for the three $M3/E2$ transitions are given in Table V.

The data analysis for three of these predominantly $E2$ γ rays presents particular problems. The 962 and 966 keV γ rays are so close together in energy that it is difficult to resolve them completely even with high-resolution Ge(Li) detectors, and the analysis for their intensities must be carried out carefully. As mentioned earlier, the spectra were analyzed during the experiment using a simple algorithm which sums the counts in the peak region and subtracts a linear background, in order to provide a running check on the results. After the experiment was completed the spectra were reanalyzed using a more sophisticated spectrum-fitting procedure (HYPERMET. For most γ rays, anisotropies obtained from the two procedures agreed within statistical errors, although the scatter (and thus the quality of the anisotropy-temperature fits) was improved in the HYPERMET results. However, in the case of the 962–966 keV doublet, the scatter of the anisotropies from the summing analysis was unacceptably large, due to the poor peak separation. The HYPERMET results yielded a "warm" intensity ratio (966/962) of 2.584(6) for the 0° detector and 2.609(3) for the 90° detector, compared with an accepted value of 2.585 (see Refs. 19 and 20). The excellent agreement lends confidence in the peak area analysis (for the warm data) using HYPERMET. An additional complication in the case of the 966 keV γ ray is the presence of a Compton edge at 967.9 keV from the strong 1178 keV transition. Figure 7 shows the anisotropy versus temperature data (HYPERMET analysis) for the 966 transition, along with the results of single- and three-parameter fits [in the latter, the free parameters were the ($L=2/L=1$) ratio R of the preceding 870 keV β branch, and the hyperfine frequencies; the single-parameter fits were performed with R as the only free parameter]. The data from the 90° detectors are seen to give relatively good agreement for the two fit methods (and strongly favor $R=0$ in both cases), while the single-parameter fit to the 0° data using the NMR frequencies shows serious deviations, especially at low temperatures; again, $R=0$ was favored. These data can be fit well by leaving the hyperfine frequencies free, but the resulting values are extremely low and were therefore not included in the weighted averages reported in Table I. The fitted values of R in this case was 0.057(3). The reason for the discrepancy in the fitted hyperfine frequencies is not clear; errors due to the 1178 keV Compton edge should be minimal, since the anisotropies of the two γ rays have the same sign and similar magnitudes, and in any case, such errors should be at least as important in the data from the 90° detector as in that from the 0° detectors. A similar argument applies to an imperfect peak separation of the 962–966 keV γ rays. The weighted average of R from the three-parameter fits is 0.009(1), so we take the upper limit to be $R<0.01$ for the 870 keV β branch (and, by arguments given in Ref. 18, similar limits should hold for the first-forbidden 680 and 787 keV β branches).

It is possible to avoid the difficulties in separating these two γ ray peaks by fitting the combined anisotropies obtained from the summed counts of both peaks. We have carried out such combined-anisotropy fits, in which the four parameters $\delta(962)$, R, ν_M, and ν_P, or the two parameters $\delta(962)$ and R, were varied. These fits are somewhat less sensitive to $\delta(962)$ due to the effect of the stronger 966 keV γ ray. The results give values for $\delta(962)$ in reasonable agreement with the fits to that transition alone (see below): $-9.1(+5.2/-2.8)$ for the 0° data and $-22(+12/-10)$ for the 90° data. The fitted hyperfine frequencies were also improved, both data sets being in good agreement with the NMR values. This improvement in the case of the 0° data is due to a cancellation of the extremely high frequencies obtained for the 962 keV γ ray by the low values obtained for the 966 keV γ ray, and is a further indication of the peak separation problem for this doublet. The 0° data favor an R value of

TABLE IV. $E2/M1$ multipole mixing ratio results for ^{160}Dy using the TDLSF, A_2, and MS methods.

E_γ (keV)	$\delta\pm\Delta\delta$	$\delta_2\pm\Delta\delta_2$	$\hat{\delta}\pm\Delta\hat{\delta}$
765	-13.66 ± 0.21	$-13.12^{+0.70}_{-0.78}$	$-13.74^{+0.79}_{-0.90}$
872	-1.08 ± 0.08	$-0.942^{+0.074}_{-0.086}$	$-0.953^{+0.081}_{-0.105}$
879	-16.6 ± 0.1	$-16.29^{+0.43}_{-0.46}$	$-16.61^{+0.47}_{-0.49}$
962	-13.04 ± 0.14	$-14.97^{+0.33}_{-0.35}$	$-13.77^{+0.32}_{-0.33}$

TABLE V. $M3/E2$ multipole mixing ratio results for ^{160}Dy using the TDLSF, A_2, and MS methods.

E_γ (keV)	$\delta\pm\Delta\delta$	$\delta_2\pm\Delta\delta_2$	$\hat{\delta}\pm\Delta\hat{\delta}$
197	$+0.0144\pm0.0028$	$+0.0208\pm0.0066$	$+0.0237\pm0.0078$
682	$+0.0067\pm0.0079$	$+0.0037\pm0.0206$	$+0.0039\pm0.0168$
1069	$+0.0033\pm0.0284$	$+0.0148\pm0.0469$	$+0.0222\pm0.0362$

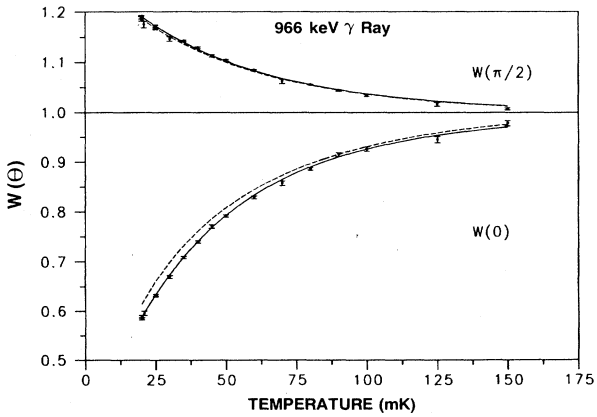

FIG. 7. $W(0)$ and $W(\frac{1}{2}\pi)$ as a function of temperature for the pure $E2$ 966 keV transition. The solid and dashed curves are weighted least-squares fits to the data (see text).

about 0.09, in agreement with that assumed in Ref. 18, while the 90° give R near 0, as do most of the other fits to the predominantly $E2$ γ rays.

Figure 8 shows the results of the HYPERMET analysis for the 962 keV γ ray for both single- and three-parameter fits. The data show considerable scatter, owing to its very small anisotropy. The latter is a result of the δ value, which gives rise to a cancellation of the F_2 coefficients (thus very small A_2) so that only the weak B_4 term contributes significantly to the anisotropy. The three-parameter fits gave hyperfine frequencies in reasonable agreement with the NMR values for the 90° data, while the magnetic hyperfine frequency was unusually high for the 0° data. The results for δ from the 0° and 90° data sets agree well, and the weighted average of δ from the two fits is $-13.04(14)$. This value is relatively insensitive to the $L=2$ ratio R of the preceding β decay; using $R=0.10$ instead of $R=0$ gives $\delta=-12.94(17)$, but the fit quality favors $R=0$.

The third γ ray for which difficulties might be expected is the $E2/M1$ transition at 765 keV. Here, again a Compton edge (from the 966 keV γ ray) underlies the peak in the γ-ray spectrum. In this case, the anisotropies of the two γ rays have opposite signs (compare Figs. 6 and 7) and rather different magnitudes. Nevertheless, fitting of both summed data and HYPERMET data yielded similar mixing ratios [$-12.49(48)$ and $-13.66(21)$, respectively, from single-parameter fits]. It thus appears that the effect of the underlying Compton edge is not serious, since the two peak-area determinations differ considerably in their abilities to separate such a background edge from the photopeak. We note that most previous determinations of the mixing ratio for this transition gave smaller values, corresponding to reduced anisotropies (this applies both to NO results and γ-γ directional correlation, $\gamma\gamma(\theta)$, measurements); this may indicate that the detectors used, with generally poorer peak-Compton ratios than in the present experiment, combined with simple peak-area algorithms, led to errors due to the 966 keV Compton edge. In particular, the reported δ values for this transition, and thus of observed anisotropy, may be seen to increase with time (see the results for this transition in the next section), paralleling the improvement in peak-Compton ratios of available Ge(Li) detectors.

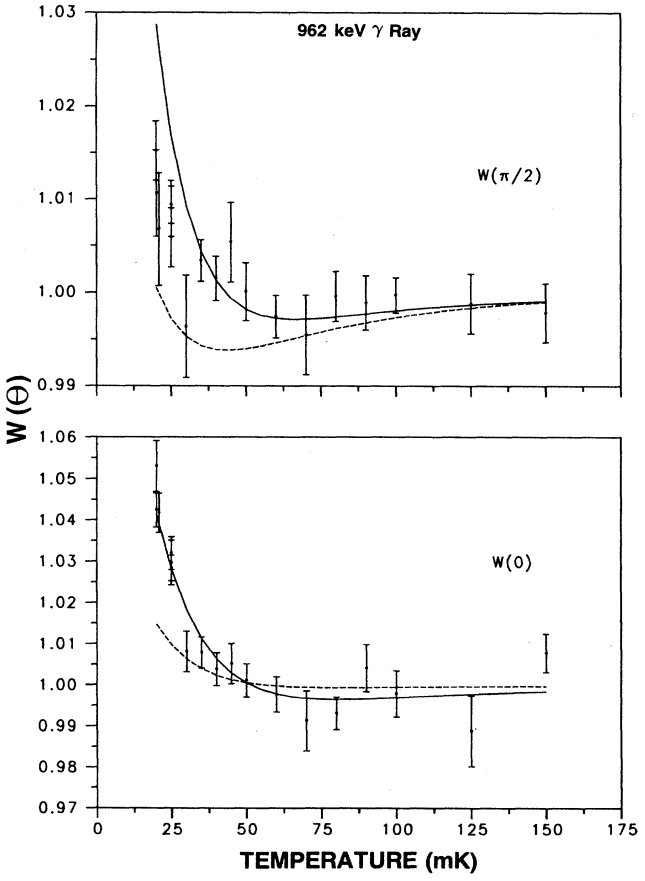

FIG. 8. $W(0)$ and $W(\frac{1}{2}\pi)$ as a function of temperature for the $E2/M1$ 962 keV transition. The solid and dashed curves are weighted least-squares fits to the data (see text).

B. Multipole mixing ratio using the A_λ and MS methods

Using the annealed NMR-ON values for the hfi parameters, along with the U_λ values given in Table II and the Q_λ values described previously, multipole mixing ratios were also determined using the A_λ and the MS methods described in Sec. IV. The weighted averages of the three runs at 25 mK ($B_2\pm\Delta B_2=0.923\,63\pm0.005\,48$ and $B_4\pm\Delta B_4=0.052\,19\pm0.003\,58$) were used to obtain $\delta_2\pm\Delta\delta_2$ by the A_2 method and $\hat{\delta}\pm\Delta\hat{\delta}$ by the MS method. These results are also given in Tables III–V. (The values given for $\Delta\delta_2$ and $\Delta\hat{\delta}$ in these tables do not include any uncertainties in the U_λ values. These are discussed at the end of this section.) The results $\delta_4\pm\Delta\delta_4$ obtained using the A_4 equation only gave real solutions for 8 of the 21 γ rays analyzed; these, in general, disagreed substantially with those obtained from the A_2 equation. As can be seen in Tables III–V the agreement between δ_2 and $\hat{\delta}$ is quite good for most of the transitions, indicating that the data points, given by $W(0)_m$ and $W(\pi/2)_m$, lie very close to their respective parameter ellipses.[23] A good example of this can be seen in the parametric plot for the intense ($I_\gamma=29.4$) $M2/E1$ 299 keV transition, Fig. 9. The data (i.e., the datum point and its errors) are so small for this transition that they cannot be seen on a normal parametric plot (where the parameter ellipse fills the entire figure), but only a magnified plot. The inset in Fig. 9 is a 55× magnification of the region around the datum point, labeled A. In addition to both sides of the parameter ellipse (dark lines), the "noncentrality" bounds (dashed lines), and constant δ values (light lines) are also shown. The "noncentrality" bounds are the error parameter ellipses which reflect the uncertainties ΔB_λ, ΔU_λ, and ΔQ_λ, and are used along with the statistical errors $\Delta W(0)_m$ and $\Delta W(\frac{1}{2}\pi)_m$ in determining the $\Delta\hat{\delta}$ values.[17] The datum point A, which lies very close to the parameter ellipse and clearly favoring small δ values, has not

been corrected for both true and random coincidence summing. When these corrections, which are quite small (less than 0.05% for this transition) are applied, the datum point (now labeled B) moves (fortuitously) even closer to the parameter ellipse. True and random summing corrections, although never more than 0.1%, were applied to all the transitions in determining δ_2 and $\hat{\delta}$.

The usefulness of parametric plots is that they not only allow the experimenter to view the data with respect to the parameter ellipse, but also they can give a simple visual representation for $\hat{\delta}$ and for the δ_λ values (as well as their errors).[17] In the MS method the value of $\hat{\delta}$ is that value of δ on the parameter ellipse which is closest to the datum point on a transformed parametric plot. The latter is a parametric plot that has been scaled such that the errors $\Delta W(0)_m$ and $\Delta W(\frac{1}{2}\pi)_m$ are exactly the same length. Thus, the value of $\hat{\delta}$ is unique except when the datum point falls on a major axis of the parameter ellipse. In this case, which is very improbable, $\hat{\delta}$ can be double or even triple valued. However, in the A_λ method there are always two solutions for both δ_2 and δ_4 since they are found by solving a quadratic equation in δ; Eq. (8) with $A_2 = A_{2m}$ and $A_4 = A_{4m}$. These solutions are just the δ values on the parameter ellipse where the A_{2m} line and A_{4m} line cut it. These lines are generated using Eqs. (12) and (13) by keeping the values of A_{2m} and A_{4m} fixed and letting $W(0)_m$ and $W(\pi/2)_m$ vary. Thus, the datum point must be exactly on the parameter ellipse for at least one of the δ_2 and one of the δ_4 solutions to be identical. (If the datum point is inside the parameter ellipse all four solutions are real, and if it is outside the solutions can sometimes be imaginary.)

In Fig. 9 we saw that the datum point B was on the inside of the parameter ellipse and almost on the upper part. Thus one would expect that one of the δ_2 solutions and one of the δ_4 solutions, along with the $\hat{\delta}$ solution to all be very close. Although both δ_2 and $\hat{\delta}$ are essentially the same (see Table III), the δ_4 solution, $+0.0762$ (and -0.0762, for mixed dipole-quadrupole transitions the δ_4 solutions are always symmetrical) is substantially different. It is only when the errors in the δ_4 solution are taken into account that it becomes consistent with the δ_2 and $\hat{\delta}$ values.

The narrowness of the parameter ellipse in Fig. 9 is typical of many of the transitions analyzed in this work (some are so narrow that they look almost like straight lines on a normal parametric plot). This narrowness comes about from the small contribution of the $\lambda=4$ term and the fact that B_2 is at only 64% of saturation at 25 mK. Not only is B_4 very small at this temperature (see Sec. II), but U_4 is also quite small for some of the transitions (see Table II). For some of the weaker transitions, although the datum point might favor one side of the parameter ellipse over the other, the errors, $\pm\Delta W(0)_m$ and $\pm\Delta W(\pi/2)_m$, overlap both sides of the ellipse. In these cases it is difficult to decide which side of

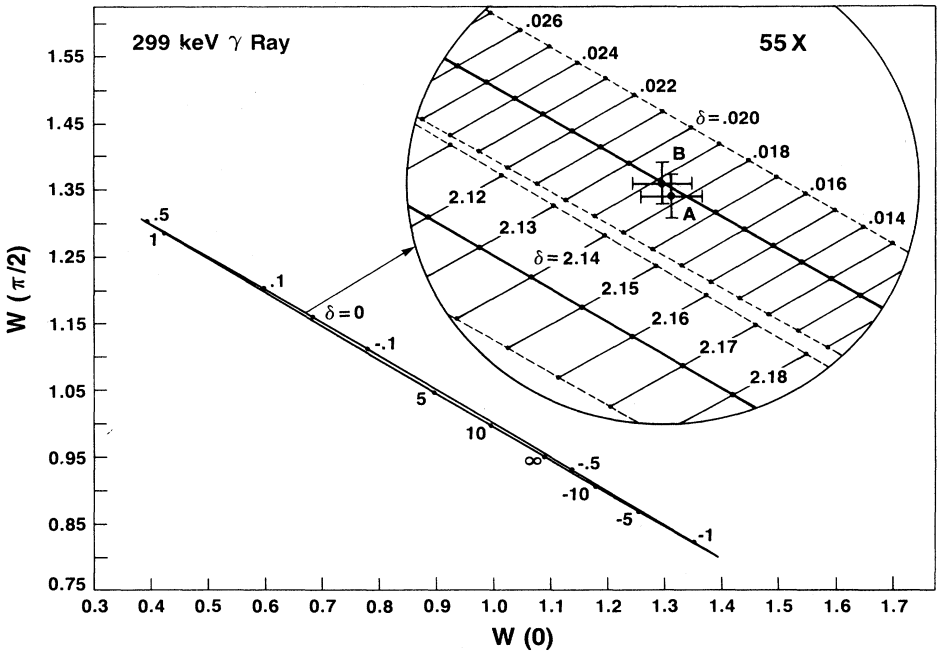

FIG. 9. Parametric plot for the $M2/E1$ 299 keV transition. The inset is a magnification (55×) of the region around the experimental data (A) showing both sides of the parameter ellipse (dark lines). After true and random coincidence summing corrections have been applied to the data it moves to B. The "noncentrality" bounds (dashed lines) and constant δ values (light lines) are also shown (see text).

the parameter ellipse is "really" closest to the datum point. This situation is depicted quite clearly in the parametric plot for the weak ($I_\gamma = 0.34$) $M2/E1$ 337 keV transition, Fig. 10. Although this parameter ellipse is one of the widest of all the transitions, the errors still overlap (see 9× magnification inset) both sides of the ellipse with the datum point favoring the upper part. On the basis of these data alone one would be forced to favor the (physically unlikely) high-δ values for this transition. In Fig. 11 we show how the parameter ellipse gets larger for this transition as we decrease the temperature. Clearly it would have been advantageous (as pointed out earlier) to have taken our (repeat runs) lowest-temperature anisotropy data at 5 mK, or even 10 mK, rather than at 25 mK as we did. (This, as we pointed out in Sec. III, was impossible using our present ^{3}He-^{4}He dilution refrigerator.) However, the data we took at 20 mK (and those at 18.8 mK with $B_{\rm app} = 0.5$ T), although statistically not as meaningful as those taken at 25 mK, can be used to decide which side of the parameter ellipse is really closest to the datum point. In this way we were able to select the correct δ values for those transitions whose parametric plots were ambiguous at 25 mK.

The parametric plot for the 337 keV transition (Fig. 10) was calculated assuming that the spin of the 1386 keV level is 4^-. We have also calculated the parametric plot for the case of spin 3^-. Not only did the datum point fit poorly on this plot, but the $\hat{\delta}$ value was unrealistically large (-0.83) for this transition which is expected to be almost pure $E1$. Since the 1103 keV transition ($I_\gamma = 0.63$), which is also expected to be almost pure $E1$, originates from the same level we again did parametric plots for the two spin cases. The results were similar to those for the 337 keV transition with $\hat{\delta} = -0.59$ when $I_1 = 3^-$. Thus we can conclude that the spin of the 1386 keV level is 4^-.

Two more results for $M2/E1$ transitions are shown in Fig. 12. In this figure (as well as the next two figures) we show only a magnified region of the parametric plot. In addition to showing both sides of the parametric ellipse, the "noncentrality bounds" and the constant δ values, we now show the $\hat{\delta}$ value (very dark line in the crosshatched area) and the range of $\pm\Delta\hat{\delta}$ (cross hatched region). As can be seen in Fig. 12(a) (55× magnification) the intense 1178 keV transition's datum point is in good agreement with the upper part (small δ values) of the parameter ellipse. In Fig. 12(b) (22× magnification) we show the excellent agreement for the less intense 1200 keV transition's datum point with the lower part (again small δ values) of the parameter ellipse.

In Fig. 13 we show results for two of the four $E2/M1$ transitions listed in Table IV. Figure 13(a) (65× magnification) shows the intense ($I_\gamma = 33.0$) 879 keV transition, whereas Fig. 13(b) (21× magnification) is for the less intense ($I_\gamma = 2.58$) 765 keV transition. Although the parameter ellipses are very narrow (the "noncentrality" bounds overlap) for both transitions, the datum point in each case favors (as expected) the large δ-value sides of the ellipses. The fact that the datum point for each lies about 1σ (standard deviation) from the "noncentrality" bounds is not abnormal. It is only when the datum point lies $> 2\sigma$ away that the analysis should be suspect. A good example of this can be seen in the results for the $E2/M1$ 962 keV transition ($I_\gamma = 10.6$), Fig. 14 (32× magnification), where the datum point is about 8σ away from the $\hat{\delta}$ value on the parameter ellipse. The results for $\hat{\delta}$ and δ_2 disagree more for this transition than for any of the other ones analyzed. As pointed out in the last section this transition could not be completely resolved from the intense ($I_\gamma = 27.3$) pure $E2$ 966 keV transition. Although HYPERMET gave excellent intensity ratios for the warm data (for both detectors) it was not able to resolve the doublet correctly in the case of the cold data; particularly so for the 0° detector, see Fig. 7. Since $\delta = 0$ for the 966 keV transition, its parameter ellipse is just a point on the $W(0)$, $W(\pi/2)$ plane.[23] The difference between it and the datum point can be used to make a crude cold count correction to the 962 keV datum point in Fig. 14. Although this correction improves the position of the datum point it cannot be taken very seriously because of the small anisotropies involved, see Fig. 14. Clearly a much more careful spectrum analysis of the 962–966 doublet (e.g., examining the anisotropy of the low part of the 966 peak and how it affects the 962 peak) has to be done before any meaningful δ value can be obtained for it. Thus, the values we give for the mixing ratio in Table IV for this transition have a large associated uncertainty which is not reflected in the errors shown.

A second (even closer) doublet is that due to the 1003–1005 keV transitions. The 1005 keV transition originates from the 1288.6 keV level which has been assigned as either 4^+ or 5^+ (see Fig. 3). In either case it is an important γ ray since its multipolarity is $E2/M1$ (thus giving us a fifth $E2/M1$ transition). Systematics would favor the 5^+ assignment since it would then be a member of the $K = 2^+$ (γ vibrational) band. The intensity of this transition has been reported by Jin *et al.*[24] to be about 0.04. However, the peak-stripping method used in their analysis is subject to a large uncertainty. (Jin *et al.* used the 1004 keV γ ray from ^{154}Eu to obtain the correct peak shape for their detector, but failed to take into account the effect of the 996 keV γ ray from the same source.) We analyzed the 1005 keV transition by assuming that its anisotropy was the same as that of the 1003 keV transition, for both spin cases. Although our results favor the 4^+ assignment with a $\hat{\delta}$ value of -0.73 (the 5^+ assignment gave $\hat{\delta} = +0.09$) they should not be taken too seriously because of the assumption we made and the lack of good intensity measurement.

As can be seen in Tables III–V, the mixing ratios obtained by the three different methods are in excellent agreement. Since those obtained using the TDLSF method make use of all of the temperature data, this agreement reflects the consistency of our temperature scale. Although one would favor the results obtained from the TDLSF method (since it uses more data to obtain its δ values), its errors ($\Delta\delta$), as mentioned earlier, do not take into account the errors in the temperature, nor in ν_M, ν_P, U_λ, and Q_λ (see Sec. IV). The MS method, in contrast, does correctly take into account the errors in the parameters listed above, as well as $\Delta W(0)_m$ and $\Delta W(\pi/2)_m$. Although the A_2 method does give good re-

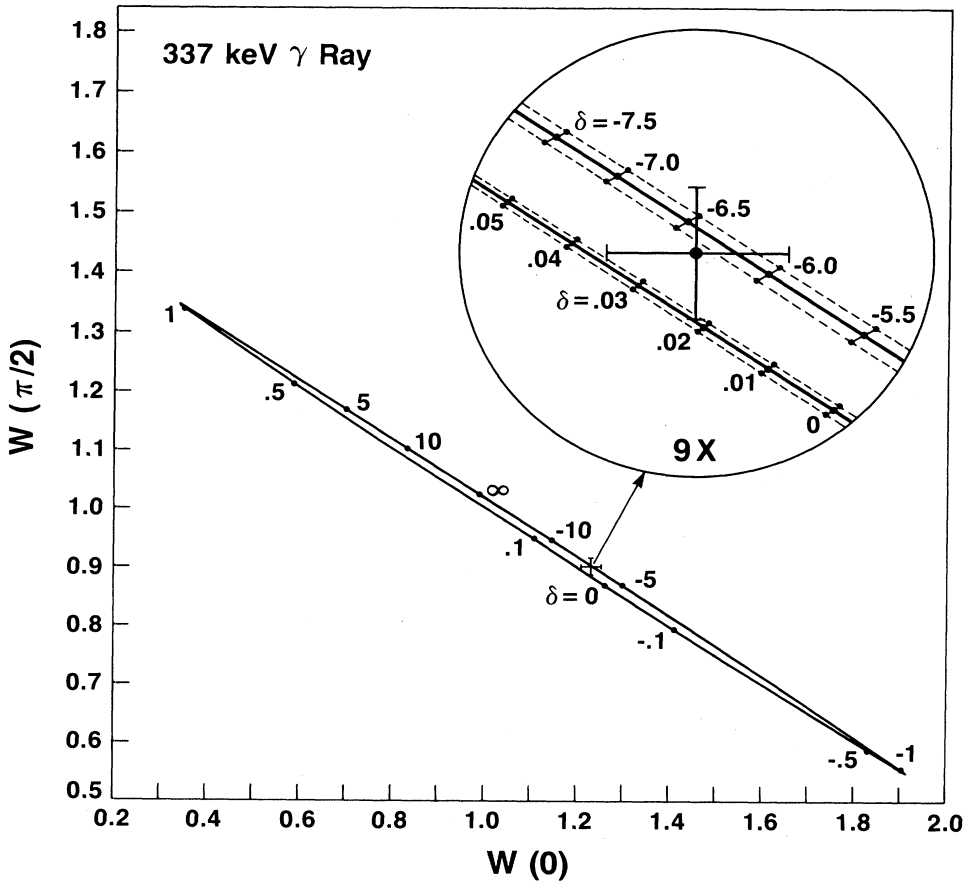

FIG. 10. Parametric plot for the $M2/E1$ 337 keV transition (see Fig. 9 and text).

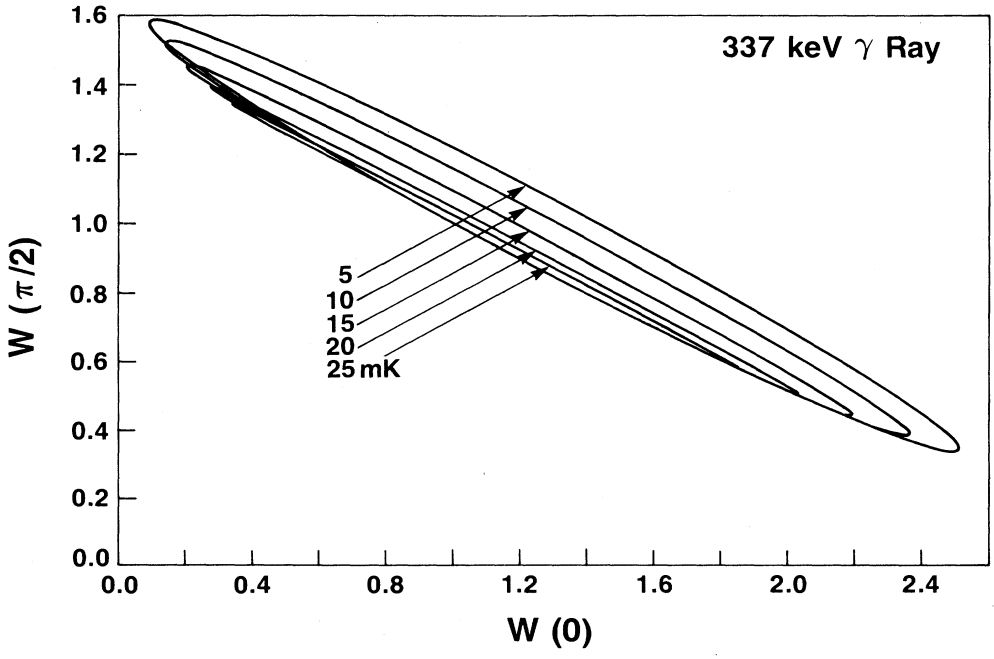

FIG. 11. Change in the parameter ellipse as a function of temperature for the $M2/E1$ 337 keV transition.

sults here (the datum point lies very close to the parameter ellipse in most cases), it is not as exact as the MS method. Finally, the MS method is also preferred over the TDLSF method when the hyperfine parameters are known, since better statistics can be acquired in a shorter time leading to more exact values for the mixing ratios. In the rest of this paper we will use only the $(\hat{\delta}\pm\Delta\hat{\delta})$ values.

As mentioned earlier, the errors $\Delta\hat{\delta}$ given in Tables III–V were obtained for $\Delta U_\lambda=0$. Assuming that this is the case for the time being, then the major contributions to $\Delta\hat{\delta}$ are from ΔB_λ (usually ΔB_2), and from $\Delta W(0)_m$ and $\Delta W(\pi/2)_m$. The contribution from the small uncertainties in Q_λ (see the beginning of this section) can essentially be ignored. For intense transitions with large anisotropies (e.g., 299, 1178, and 172 keV) the contribution

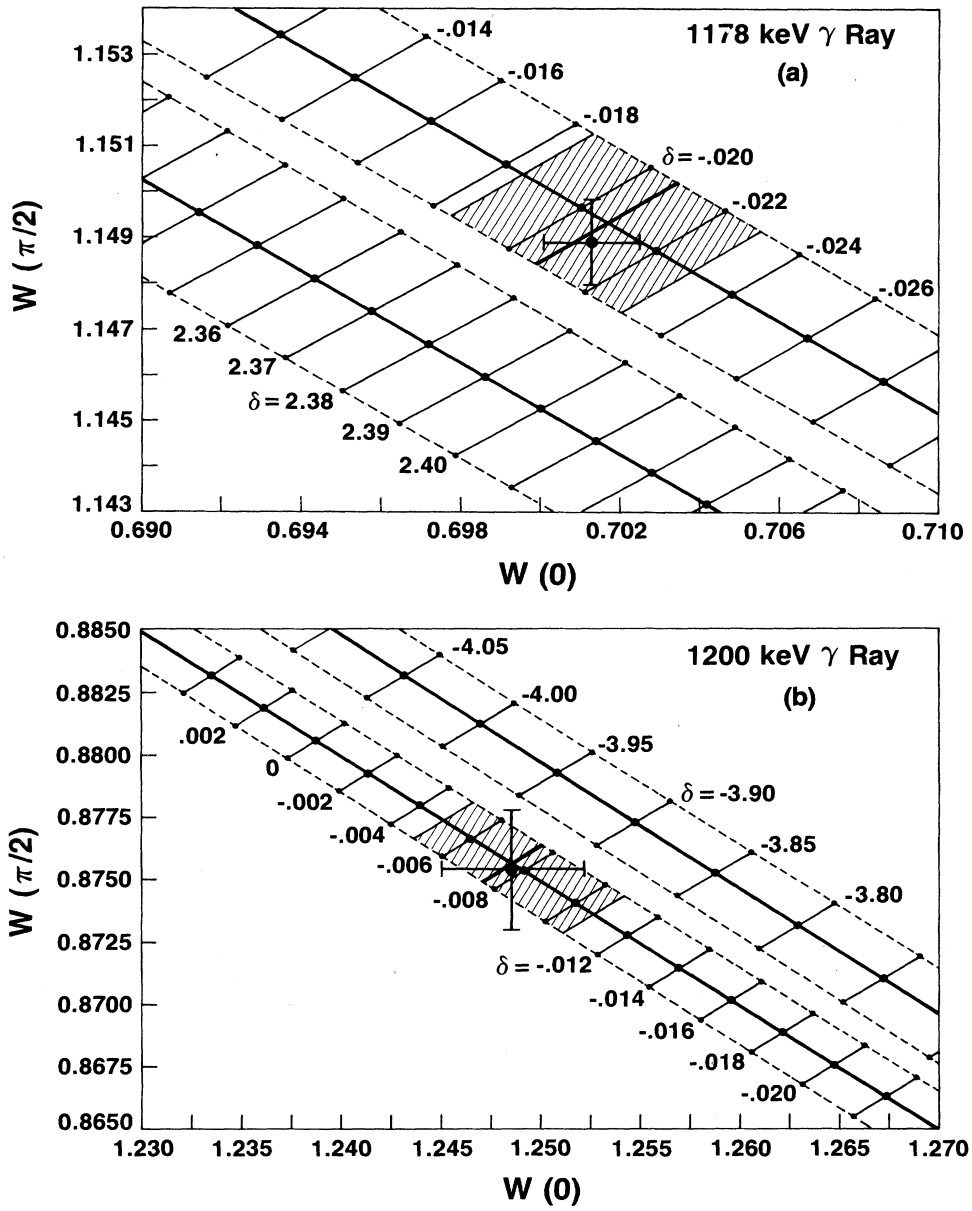

FIG. 12. Magnified regions of the parametric plots for the 1178 and 1200 keV $M2/E1$ transitions. In addition to showing both sides of the parameter ellipse (dark lines), the "noncentrality" bounds (dashed lines) and the constant δ values (light lines), we now show the $\hat{\delta}$ value (very dark line in the crosshatched area) and the range of $\pm\Delta\hat{\delta}$ (crosshatched area).

to $\Delta\hat{\delta}$ from ΔB_2 is about equal to those from $\Delta W(0)_m$ and $\Delta W(\pi/2)_m$. (The major source of the error in B_2 is that from the $\pm 1\%$ uncertainty in the temperature scale. At 25 mK, ΔT is responsible for 91.6% of the error in B_2, while $\Delta\nu_M$ for 3.9% and $\Delta\nu_P$ 4.5%.) For weaker transitions (e.g., 393 and 1312 keV), or those with smaller anisotropies (e.g., 765 and 879 keV), $\Delta W(0)_m$ and $\Delta W(\pi/2)_m$ are responsible for the major part of $\Delta\hat{\delta}$. The errors in U_2 and U_4 are caused by uncertainties in the relative intensities, in some cases by small admixtures ($L=0$ and 2) in the β feeding, and admixtures in some of the γ feeding. For example, if we had 20% $L=0$ admixture in the β feeding of the 1398.9 keV level, the $\hat{\delta}$ value for the 1312 keV γ ray would change from -0.0149 to -0.0123, i.e., a change of about 17%, which is slightly less than the error $\Delta\hat{\delta}$. Although some of the levels (e.g., 1535.2, 1358.7, and 1398.9 keV) have little or no uncertainties in U_λ from admixtures in the γ feeding, others

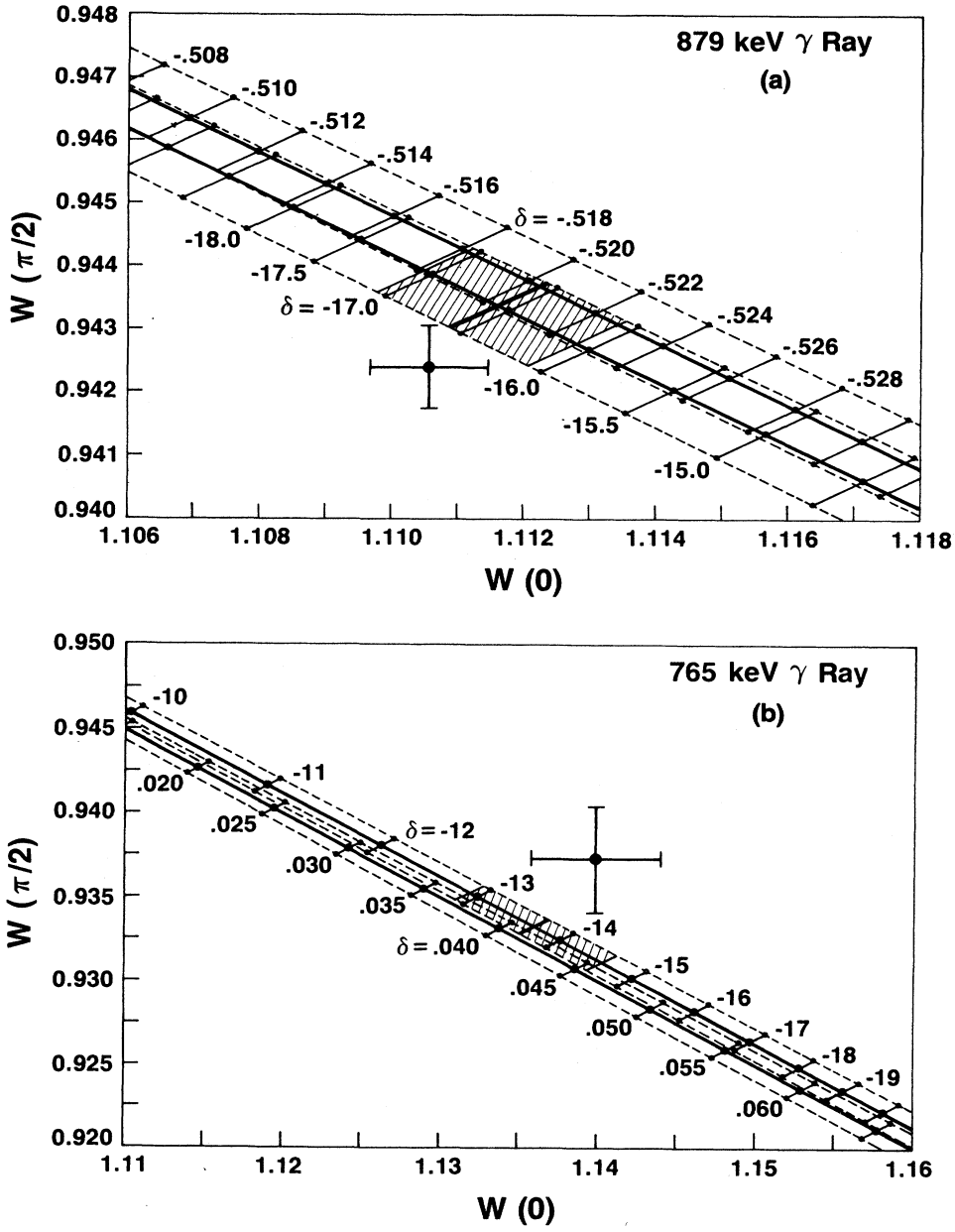

FIG. 13. Magnified regions of the parametric plots for the 765 and 879 keV $E2/M1$ transitions (see Fig. 12 and text).

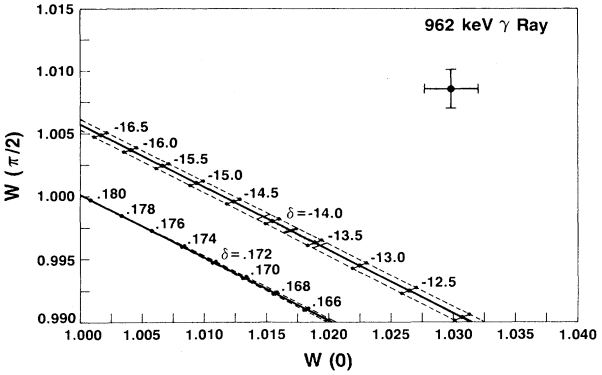

FIG. 14. Magnified region of the parametric plot for the $E2/M2$ 962 keV transition (see Fig. 12 and text).

(e.g., 1049.1 and 966.2 keV) could have as much as 1–2 %. Since $\Delta U_\lambda/U_\lambda$ enters into the error equation[17] for $\Delta\hat{\delta}$ in the same way as $\Delta B_\lambda/B_\lambda$, a ±1% error in U_2 essentially doubles the error due to ΔB_2 [note; $(\Delta B_2/B_2)=0.6\%$]. For example, for the 299 keV transition a ±1% error in U_λ would increase $\Delta\hat{\delta}$ from ±0.0024 to ±0.0046, whereas for the 879 keV transition $\Delta\hat{\delta}$ would go from +0.47/−0.49 to +0.66/−0.70. The only other source of uncertainty in $\hat{\delta}$ is that from using the unannealed NMR hfi values for ν_M and ν_P instead of the annealed ones (see Table I). This would only change $\hat{\delta}$ by a few percent, e.g., $\hat{\delta}$ for the 299 and 879 keV transitions would be 8.8% and 1.2% lower, respectively.

VI. DISCUSSION

In Table VI we compare our results for the $M2/E1$ mixing ratios with those from three other NO studies done in ^{160}Tb. The measurements of Krane[18] were made using polycrystalline terbium metal with the ^{160}Tb produced *in situ* by neutron activation, whereas Gromova *et al.*[25] and Fox *et al.*[26] incorporated the ^{160}Tb in gadolinium metal (by melting). As can be seen, the results of Gromova *et al.*[25] are in better agreement with ours than either of the other two. This is no doubt due to their having used better values for the hfi parameters. They determined the hfi parameters for ^{160}Tb*Gd* by fitting the measured anisotropies of the 299 and 1178 keV γ rays. Their results were in good agreement with those of Erzinkyan *et al.*[27] on the same system, as well as those deduced from the NMR results on ^{159}Tb*Gd* by Kobayashi *et al.*[28] The hfi parameters used in the earlier work by Fox *et al.*[28] were not in good agreement with the above results (their dipole and quadrupole interactions were about 10 and 100 % higher, respectively). Krane[18] obtained by hfi parameters for ^{160}Tb*Tb* by setting the dipole splitting $\Delta_M=65$ mK and determining $\Delta_P(=-2\pm2$ mK) from the measured anisotropies of some of the more intense transitions. These values are lower than ours (see Sec. II), which could be due to incomplete magnetic saturation of his polycrystalline sample.

As can be seen in Table VI our values for the 14

TABLE VI. ^{160}Dy $M2/E1$ multipole mixing ratios. Comparison with other NO measurements.

E_γ (keV)	This work	Krane[a]	Gromova *et al.*[b]	Fox *et al.*[c]
216	+0.0046(53)	−0.010(9)	+0.016(8)	−0.003(6)
299	+0.0188(24)	−0.024(14)	+0.023(18)	−0.011(29)
310	−0.0134(72)	−0.025(25)	−0.06(3)	−0.020(44)
337	+0.0284(128)	−0.006(33)	+0.034(27)	+0.039(32)
393	+0.0181(57)	−0.016(16)	−0.018(17)	−0.043(15)
486	+0.0357(287)			
1003	+0.0010(49)	−0.009(15)	+0.094(21)	−0.004(17)
1103	+0.0049(121)	−0.085(40)	−0.013(46)	−0.156(25)
1115	+0.0012(32)	−0.013(8)	+0.011(14)	0.000(12)
1178	−0.0207(23)	−0.062(4)	−0.015(8)	−0.031(12)
1200	−0.0077(29)	+0.026(5)	−0.050(11)	−0.017(8)
1251	−0.0058(312)	−0.118(85)	$+0.02^{+0.19}_{-0.12}$	
1272	+0.0166(25)	−0.029(5)	+0.026(9)	−0.003(12)
1312	−0.0149(28)	+0.013(6)	−0.045(11)	−0.017(8)

[a]Reference 18.
[b]Reference 25.
[c]Reference 26.

$M2/E1$ mixing ratios from the negative-parity levels are quite small, all being close to zero as expected. However, some of them are larger than their single-particle estimate. Günther *et al.*[29] showed that the energies of the negative-parity states in ^{160}Dy could be accounted for quite well by Coriolis mixing of the $K=0$, 1, and 2, bands. Their band-mixing calculation was also fairly consistent with the relative $E1$ transition probabilities from the negative-parity levels to both the ground-state ($K=0^+$) and γ-vibrational ($K=2^+$) bands. Krane[18] examined whether this band-mixing calculation could also be consistent with the measured values for the mixing ratios. Since he has discussed this calculation in considerable detail we will only give his results here (his notation will be used). He showed that the reduced $M2/E1$ mixing ratios for transitions to the $K=2^+$ band can be given by

$$\Delta(E_\gamma)=a_1S_1'+a_2S_2' , \tag{15}$$

where S_1' and S_2' are the $M2/E1$ matrix element ratios for the intrinsic system. These are independent of the spins of the initial and final states and should be the same for all the transitions to the 2^+ band. The quantities a_1 and a_2 are different for each transition since they depend upon the spins of the initial and final states as well as on the energies of the negative-parity levels. Thus, by least-squares fitting the measured mixing ratios for all the transitions to the 2^+ band, values for S_1' and S_2' can be obtained and used to deduce fitted mixing ratios. In order to determine S_1' and S_2' Krane[18] did not use his own δ values, but averaged his results with those of Gromova *et al.*[25] and Fox *et al.*[26] [Before doing this he reanalyzed their data using $\delta(299)=-0.014(4)$. He obtained this value by averaging the three NO results for this transition with the $\gamma\gamma(\theta)$ results of Bhati *et al.*,[30] Gardulski and Widenbeck,[31] Krane and Steffan,[32] Jaklevic *et al.*,[33]

and also with the $\gamma\gamma(\theta)$ and e_K-γ directional correlation, $e_K\gamma(\theta)$, result of Zawislak *et al.*[34]] The resulting measured reduced mixing ratios, Δ_m [here expressed in units of μ_N/e and obtained using $\Delta_m=\delta/-9.23\times10^{-5}\ E_\gamma$ (MeV)] are given in Table VII along with the values deduced for Δ_{fit} (the fitted reduced mixing ratios), S'_1, S'_2, and the reduced chi squared, χ^2_ν. (The values given here for Δ_{fit}, S'_1, and S'_2 are slightly different from those given by Krane[18] as we redid the least-squares fitting using his Δ_m values in order to obtain χ^2_ν.) Krane[18] concluded that the agreement between the measured and fitted values was not satisfactory. We have carried out a similar analysis for the same transitions using our values for the mixing ratios and the results are also given in Table VII. As can be seen, the agreement is also very poor ($\chi^2_\nu \gg 1$). We also redid the calculation including the 486 keV transition; the results were only slightly better. Thus we must conclude that this band-mixing calculation cannot explain the $M2/E1$ mixing ratios for transitions from the negative-parity levels to members of the $K=2^+$ band.

Krane[18] carried out a similar analysis for the transitions from the negative-parity levels to the ground-state band. In this case the expression is

$$\Delta(E_\gamma)=a_1S''_1+a_2S''_2\ . \tag{16}$$

In Table VIII we give results for Δ_{fit}, S''_1, S''_2, and χ^2_ν using both his and our Δ_m values. Krane[18] concluded here that the agreement between his Δ_m values and the deduced Δ_{fit} values was quite good. He noted that the phases were given correctly for seven of the eight transitions and, except for the 1103 and 1251 keV transitions (which are the weakest), the overall magnitudes were in good agreement. As can be seen in Table VIII, our values for Δ_m are quite different from his and the deduced Δ_{fit} values are in slightly better agreement (the χ^2_ν value is smaller for our data). However, the χ^2_ν values for both sets of data are too large to inspire confidence in either fit. In Fig. 15 we show the Δ_m values and their errors along with the Δ_{fit} values for both his [Fig. 15(b)] and our [Fig. 15(a)] data. Krane[18] suggested that the Δ_m value for the 1103 keV transition could be in error and disregarding it would improve the quality of the fit (redoing the fit without it results in a χ^2_ν of 2.08). We could also improve the fit to our data by eliminating the worst point (the 1312 keV transition), which would result in a χ^2_ν of 1.60. Although both sets of data now give more reasonable values for χ^2_ν, it would be impossible for both of them to substantiate this band-mixing calculation since their Δ_m values are so different. Thus, we are forced to conclude that Coriolis mixing of the $K=0,1$, and 2 bands does not explain the small values of the measured $M2/E1$ mixing ratios.

TABLE VII. Measured and fitted reduced $M2/E1$ mixing ratios of transitions from negative-partiy levels to the $K=2^+$ band in ^{160}Dy.

E_γ (keV)	Δ_m This work	Δ_{fit}	Δ_m Krane[a]	Δ_{fit}
216	−231(266)	+755	+201(201)	−135
299	−681(87)	−263	+507(145)	−63
310	+468(252)	+509	+979(384)	−91
337	−913(412)	+666	−1125(514)	−306
393	−499(157)	−254	+1020(248)	+832
χ^2_ν	17.99		9.71	
S'_1	+2636(2935) μ_N/e		−3342(3044) μ_N/e	
S'_2	+4938(4141) μ_N/e		−881(3327) μ_N/e	

[a]Reference 18.

TABLE VIII. Measured and fitted reduced $M2/E1$ mixing ratios of transitions from negative-parity levels to the $K=0^+$ band in ^{160}Dy.

E_γ (keV)	Δ_m This work	Δ_{fit}	Δ_m Krane[a]	Δ_{fit}
1003	−11(53)	+27	−140(97)	−92
1103	−48(119)	+148	+1326(177)	+106
1115	−12(31)	+48	+78(58)	−69
1178	+190(21)	+177	+110(64)	+202
1200	+70(26)	+49	−99(36)	−51
1251	+50(270)	−132	+805(580)	+104
1272	−141(21)	−144	+213(34)	+199
1312	+123(23)	0	−8(33)	−44
χ^2_ν	6.21		10.15	
S''_1	−9.22(4.07) μ_N/e		+19.27(8.72) μ_N/e	
S''_2	−5.56(1.24) μ_N/e		−0.04(3.79) μ_N/e	

[a]Reference 18.

In addition to comparing our results for the $M2/E1$ mixing ratios with those obtained from other NO experiments, we can also compare some of them with the results from the $\gamma\gamma(\theta)$ and $e_K\gamma(\theta)$ measurements[30–34] mentioned earlier. Because of the coincidence requirement in this type of measurement only favorable cascades (those with sufficient intensity) can be studied. In Table IX we give the results for the $M2/E1$ transitions from Refs. 30–34 along with our results. As can be seen there is very little agreement between our $\hat{\delta}$ values and those from the $\gamma\gamma(\theta)$ measurements. In particular three of the four $\gamma\gamma(\theta)$ results for the 299 keV transition (which is measured in coincidence with the pure $E2$ 966 keV transition) are different in sign (negative) from our result. Krane and Steffan's[32] value, although slightly positive, is not inconsistent with δ being negative. The $e_K\gamma(\theta)$ and $\gamma\gamma(\theta)$ results of Zawislak *et al.*,[34] which is definitely positive, could be in error (see Ref. 18). All the $\gamma\gamma(\theta)$ results for the 1178 and 1272 keV transitions (each measured in coincidence with the pure $E2$ 87 keV transition) are also different in sign from our NO results. Krane[18] has suggested that the small differences in δ between the $\gamma\gamma(\theta)$ and NO results could be explained by including a small $E3$ admixture, i.e., by considering triple multipole mixing ($E1+M2+E3$). In this case the expressions for the angular correlation coefficient [Eq. (8)] and the angular

TABLE IX. ^{160}Dy $M2/E1$ multipole mixing ratios. Comparison of our NO results with those from $\gamma\gamma(\theta)$ and $e_K\gamma(\theta)$ measurements.

216 keV	299 keV	393 keV	1178 keV	1272 keV	Reference
+0.0046(53)	0.0188(24)	+0.0181(57)	−0.0207(23)	+0.0166(25)	This work (NO)
	−0.048(24)				Bhati *et al.* (Ref. 30), $\gamma\gamma(\theta)$ (1976)
	−0.021(7)		+0.047(21)	−0.003(26)	Gardulski *et al.* (Ref. 31), $\gamma\gamma(\theta)$ (1973)
−0.18(10)	+0.005(10)	+0.005(70)	+0.02(2)	−0.03(3)	Krane *et al.* (Ref. 32) $\gamma\gamma(\theta)$ (1971)
−0.199(49)	−0.02(2)		+0.040(43)	−0.063(78)	Jaklevic *et al.* (Ref. 33), $\gamma\gamma(\theta)$ (1967)
	+0.04(1)				Zawislak *et al.* (Ref. 34), $\gamma\gamma(\theta)$, $e_K\gamma(\theta)$ (1973)
−0.195(44)	−0.015(5)[a]	+0.005(70)	+0.034(14)	−0.017(19)	$\gamma\gamma(\theta)$ averages

[a]Reference 34 is not included.

orientation coefficient [used in the $\gamma\gamma(\theta)$ analysis and identical to A_λ except for a phase factor] are more involved as they now contain terms in the mixing ratios $\delta_{12}(M2/E1)$ and $\delta_{13}(E3/E1)$. Since δ_{12} and δ_{13} are expected to be small for the transitions under discussion, terms in δ_{12}^2, δ_{13}^2, and $\delta_{12}\delta_{13}$ can be ignored and the resulting two expressions solved simultaneously to obtain values for δ_{12} and δ_{13}. In Table X we give the results of this analysis for the 299, 1178, and 1272 keV transitions using the average $\gamma\gamma(\theta)$ δ values and our NO $\hat{\delta}$ values from Table IX. The results for all three transitions are essentially the same; namely much larger $E3$ than $M2$ admixtures, with the latter being almost zero. Krane's[18] δ_{12} and δ_{13} values for the 1178 and 1272 keV transitions are quite different from ours since his NO δ values were different. He did not obtain any results for the 299 keV transition since his NO δ value for this transition (as mentioned earlier) was obtained by averaging all of the $\gamma\gamma(\theta)$ and NO data together. Although some $B(E3)$ values have been measured[35,36] for some of the levels in ^{160}Dy, no information is available for the two levels (1358 and 1265 keV) that feed these three transitions. Thus, until some new measurements can substantiate our results in Table X they should be viewed with caution, particularly in light of the large errors associated with the individual δ values obtained using the $\gamma\gamma(\theta)$ method.

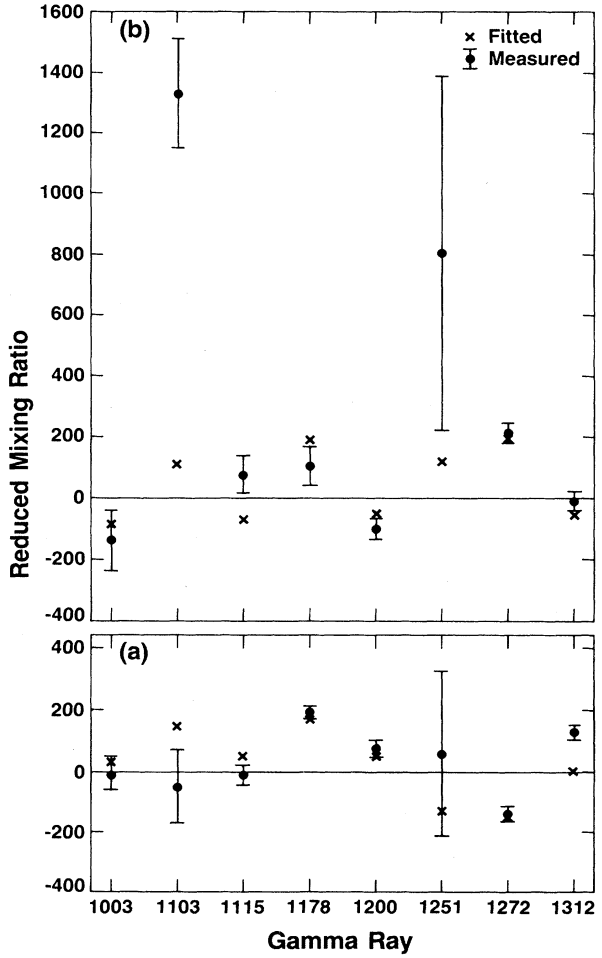

FIG. 15. Measured and fitted $M2/E1$ reduced mixing ratios of transitions from negative-parity levels to the ground-state band. The fitted values are from a band-mixing calculation (see text and Ref. 18). The upper part (b) is Krane's data (Ref. 18) and the lower part (a) is the present work.

Turning now to the $E2/M1$ mixing ratios, in Table XI we show our results for the four $\gamma\rightarrow g$ (γ vibrational to the ground-state band) transitions along with the results obtained from both NO (Refs. 18, 25, and 26) and $\gamma\gamma(\theta)$ (Refs. 30–34 and 37) measurements. Except for the 765 keV transition, the overall agreement between our results and all the others is quite good. In particular, our result for the intense 879 keV transition is in excellent agreement with that of Krane[18] as well as with most of the other values reported. The results for the 962 keV transition are also reasonably consistent. (The value of Gromova *et al.*[25] was reported incorrectly in their paper.[18] The δ value shown in Table XI was recalculated using their

TABLE X. $E3/E1$ and $M2/E1$ mixing ratios for some transitions in ^{160}Dy determined from NO and $\gamma\gamma(\theta)$ measurements.

E_γ (keV)	δ_{12}	δ_{13}
299	+0.002(4)	−0.018(4)
1178	+0.006(8)	+0.028(8)
1272	−0.000(10)	−0.018(11)

TABLE XI. ^{160}Dy $E2/M1$ multipole mixing ratios for transitions from the γ vibrational ($K=2^+$) to the ground-state ($K=0^+$) band. Comparison of NO and $\gamma\gamma(\theta)$ measurements.

879 keV ($2^{+\prime}\rightarrow 2^+$)	962 keV ($3^{+\prime}\rightarrow 2^+$)	765 keV ($3^{+\prime}\rightarrow 4^+$)	872 keV ($4^{+\prime}\rightarrow 4^+$)	Reference
$-16.61^{+0.47}_{-0.49}$	$-13.77^{+0.32}_{-0.33}$	$-13.74^{+0.79}_{-0.90}$	$-0.953^{+0.081}_{-0.105}$	This work (NO)
$-16.7^{+1.3}_{-1.6}$	-11.0 ± 1.2	$-8.3^{+0.7}_{-0.9}$		Krane (Ref. 18), NO (1982)
-12.8 ± 1.5	-37^{+17}_{-109}[a]	$-9.0^{+2.4}_{-5.0}$	-0.70 ± 0.30	Gromova *et al.* (Ref. 25), NO (1979)
-18^{+4}_{-8}		$-7.7^{+0.6}_{-0.7}$		Fox *et al.* (Ref. 26), NO (1974)
-14.5 ± 1.5	$-8.4^{+1.7}_{-2.7}$			Bhati *et al.* (Ref. 30), $\gamma\gamma(\theta)$ (1976)
-16.3 ± 1.3				Gardulski *et al.* (Ref. 31), $\gamma\gamma(\theta)$ (1973)
-11.5 ± 1.9	-18 ± 5	-7^{+5}_{-20}		Krane *et al.* (Ref. 32), $\gamma\gamma(\theta)$ (1971)
	$-9.0^{+1.7}_{-2.8}$	$-4.7^{+1.7}_{-5.0}$		Lange (Ref. 37), $\gamma\gamma(\theta)$ (1971)
-11^{+3}_{-13}	$-7.9^{+2.4}_{-6.1}$			Jaklevic *et al.* (Ref. 33), $\gamma\gamma(\theta)$ (1970)

[a]See text.

specimen five results.) The discrepancies in the δ values for the 765 keV transition could be due to the effect of the Compton edge from the 966 keV transition as explained in the last section. Although our $\hat{\delta}$ value for the 872 keV transition is in good agreement with the only other measurement reported, there are reasons to believe that it could be wrong. This is a very weak transition ($I_\gamma=0.2$) and is no doubt affected by the close and intense ($I_\gamma=33.0$) 879 keV transition; the situation is somewhat similar to that of the 962–966 keV doublet discussed earlier (but without the added complication of the Compton edge).

The interacting-boson approximation (IBA) has been very successful in describing collective properties in medium-heavy even-even nuclei. Warner[38] has shown that both the sign and magnitude of most of the measured $E2/M1$ mixing ratios of rare-earth nuclei can be accounted for reasonably well using the simplest version of this model (IBA-1, where no distinction is made between neutrons and protons). He has shown that using the IBA-1 $M1$ operator, the reduced $E2/M1$ mixing ratios for both $\gamma\rightarrow g$ and $\gamma\rightarrow\gamma$ (intraband) transitions can be given by a rather simple expression, namely

$$\Delta(E2/M1)=-1Bf(I_i,I_f)\ , \tag{17}$$

where B is a constant of the $M1$ operator and $f(I_i,I_f)$ is a spin factor given by

$$f(I_i,I_f)=[\tfrac{1}{40}(I_i+I_f+3)(I_i-I_f+2)\times(I_f-I_i+2)(I_i+I_f-1)]^{1/2}\ . \tag{18}$$

Since the spin factor is always positive, the sign of the mixing ratios is uniquely determined by the sign of B. Krane,[39] and more recently Lange *et al.*,[1] have shown that the signs of most of the measured $\gamma\rightarrow g$ $E2/M1$ mixing ratios in this mass region are negative, thus implying that the sign of B is positive. As can be seen in Table XI our results (as well as all the other results) for the four $\gamma\rightarrow g$ transitions are also negative. Warner[38] has analyzed the $\gamma\rightarrow\gamma$ transitions in ^{154}Gd, ^{162}Dy, ^{166}Er, and ^{168}Er, and found that the mean value of B was 0.042(10), 0.044(10), 0.023(5), and 0.026(1), respectively. (These mean values were based on only 1, 3, 3, and 3, intraband transitions, respectively.) Since no similar data on intraband transitions in ^{160}Dy exist, we are limited to examining the constancy of B based on our four measured $\gamma\rightarrow g$ mixing ratios. In Table XII we show the results of this calculation [here the reduced mixing ratios are obtained using $\Delta(E2/M1)=\hat{\delta}(E2/M1)/0.835E_\gamma$ (MeV)]. As can be seen, the values of B for the 879, 962, and 765 keV transitions are in rough agreement and not too different from the B values obtained above; however, the value of B for the 872 keV transition is about an order of magnitude different. As we mentioned earlier our $\hat{\delta}$ value for

TABLE XII. Values of the constant B of the IBA $M1$ operator (Ref. 38) deduced from the $E2/M1$ mixing ratios of ^{160}Dy obtained in this work.

$I_i^\pi\rightarrow I_f^\pi$	E_γ (keV)	$\hat{\delta}$ $(E2/M1)$	Δ $(E2/M1)$	f (I_i,I_f)	B
$2^{+\prime}\rightarrow 2^+$	879	$-16.61^{+0.47}_{-0.49}$	$-22.63^{+0.64}_{-0.66}$	1.449	$+0.0305\pm0.0009$
$3^{+\prime}\rightarrow 2^+$	962	$-13.77^{+0.32}_{-0.033}$	$-17.14^{+0.40}_{-0.41}$	1.549	$+0.0377\pm0.0009$
$3^{+\prime}\rightarrow 4^+$	765	$-13.74^{+0.79}_{-0.90}$	$-21.51^{+1.24}_{-1.41}$	2.121	$+0.0219\pm0.0014$
$4^{+\prime}\rightarrow 4^+$	872	$-0.953^{+0.081}_{-0.105}$	$-1.31^{+0.11}_{-0.14}$	2.775	$+0.275^{+0.025}_{-0.026}$

the 872 keV transition is subject to uncertainty. Assuming that $B \simeq 0.03$ for ^{160}Dy then we should have measured a mixing ratio of about -9 for this transition; such a value would be obtained if our $W(0)_m$ and $W(\pi/2)_m$ values were in error by $+5\%$ and -5%, respectively. These errors are not unreasonable in view of our earlier remarks about the effect of the intense 879 transition on this weak transition. [The $+5\%$ and -5% errors correspond to approximately two standard deviations; $W(0)_m \pm \Delta W(0)_m$ and $W(\frac{1}{2}\pi)_m \pm \Delta W(\frac{1}{2}\pi)_m$ are 1.185 ± 0.022 and 0.905 ± 0.021 for the 872 keV transition, respectively.] Thus, until better measurements are made on this weak transition, the disagreement between it and IBA-1 cannot be taken too seriously.

As expected, our mixing ratios for the three $M3/E2$ transitions (see Table V) are all quite small and, with the exception of the 197 keV transition, are not inconsistent with values of zero. Although Krane,[19] Gromova *et al.*,[25] and Fox *et al.*[26] have measured anisotropies for the 197 keV transition (Krane[18] also measured anisotropies for the 682 keV transition), none of them reported mixing ratios.

VII. SUMMARY AND CONCLUSIONS

In this paper we have shown that the NO technique can be used to obtain accurate values of multipole mixing ratios. The three methods currently in use for extracting mixing ratios from NO experiments were used to analyze the data and shown to agree quite well when careful measurement techniques (e.g., accurate absolute thermometry, high-resolution detectors, and a stable counting system) are employed. However, of the three, the statistical MS method gives the most meaningful value for the mixing ratio and its uncertainty. Our results for ^{160}Dy have been compared with those obtained from other NO measurements as well as those from $\gamma\gamma(\theta)$ measurements. In the case of the $E2/M1$ mixing ratios the agreement is quite good; however, for the $M2/E1$ transitions only the NO results of Gromova *et al.*[25] agree reasonably well with ours. The 14 $M2/E1$ mixing ratios that we measure (all transitions from negative-parity levels to the γ and ground-state bands) are all quite small, as expected, and cannot be explained by Coriolis mixing of the $K=0$, 1, and 2 bands. The small differences between our results for three $M2/E1$ transitions (299, 1178, and 1272 keV) and those obtained from $\gamma\gamma(\theta)$ measurements could possibly be attributed to small $E3$ admixtures. The signs (all negative) and magnitudes of the four $E2/M1$ transitions that we measured are in good agreement (except for the magnitude of the weak 872 keV transition) with the predictions of IBA-1.

Although most of the mixing ratios reported here are fairly precise, problems still exist with partially resolved peaks (e.g., the 962–966 and 872–879 doublets). These problems could be avoided by using better detectors with even higher resolution (and better peak-Compton ratios) than the ones we used, which were about ten years old. Finally, in order to provide theorists with better data to test their models [i.e., IBA-2, EPM (extended phonon projection) and other geometric and algebraic models] more, and more accurate, values of mixing ratios must be determined by NO, $\gamma\gamma(\theta)$, and other methods.

ACKNOWLEDGMENTS

We gratefully appreciate the programming help of A. N. Heckert and the technical assistance of R. B. Dove and W. J. Bowers. We also thank Dr. D. D. Hoppes, Dr. E. Bromberg, Dr. B. W. Rust, Dr. J. J. Filliben, and Dr. M. Böttcher for helpful discussions. The initial calibration of the superconducting fixed-point device by Dr. J. C. Colwell is gratefully acknowledged.

[1] J. Lange, K. Kumar, and J. H. Hamilton, Rev. Mod. Phys. **54**, 119 (1983).
[2] W. C. Koehler, in *Magnetic Properties of Rare Earth Metals,* edited by R. J. Elliott (Plenum, London, 1972), p. 81.
[3] P. Roman, W. D. Brewer, E. Klein, H. Marshak, K. Freitag, and P. Herzog, Phys. Rev. Lett. **56**, 1976 (1986).
[4] H. Marshak, W. D. Brewer, P. Roman, E. Klein, K. Freitag, and P. Herzog, Phys. Rev. Lett. **59**, 1764 (1987).
[5] W. van Rijswijk, F. G. van den Berg, W. R. Joosten, and W. J. Huiskamp, Hyperfine Interact. **15-16**, 325 (1983).
[6] P. Herzog, U. Daemmrich, K. Freitag, C. D. Herrman, and K. Schloesser, Hyperfine Interact. **22**, 167 (1985).
[7] K. H. Ebeling, R. Eder, E. Hagn, E. Zech, and M. Deicher, Phys. Rev. Lett. **54**, 2135 (1985).
[8] W. D. Brewer, P. Roman, M. Böttcher, B. Illerhaus, H. Marshal, K. Freitag, and P. Herzog, Phys. Rev. B **38**, 11 019 (1988).
[9] H. Marshak, P. Roman, and W. D. Brewer, Hyperfine Interact. **49**, 741 (1989).
[10] J. J. Rhyne, in *Magnetic Properties of Rare Earth Metals,* edited by R. J. Elliott (Plenum, London, 1972), p. 129.
[11] H. Marshak and B. G. Turrell, Solid State Commun. **30**, 677 (1979); B. G. Turrell and H. Marshak, Hyperfine Interact. **11**, 205 (1981).
[12] R. J. Soulen and R. B. Dove, Natl. Bur. Stand. (U.S.) Spec. Pub. No. 260-262 (U.S. GPO, Washington, D.C., 1979).
[13] J. H. Colwell, W. E. Fogel, and R. J. Soulen, in *Proceedings of the 17th International Conference on Low Temperature Physics,* edited by U. Eckern, A. Schmid, and H. Wuhl (North-Holland, Amsterdam, 1984), Pt. 1, p. 395.
[14] H. Marshak, in *Low Temperature Nuclear Orientation,* edited by N. J. Stone and H. Postma (North-Holland, Amsterdam, 1986), Chap. 16, p. 769.
[15] This is discussed in greater detail in a preliminary report: H. Marshak, W. D. Brewer, and P. Roman, Hyperfine Interact. **43**, 363 (1988).
[16] G. W. Phillips and K. W. Marlow, Nucl. Instrum. Methods **137**, 525 (1976).
[17] H. Marshak and C. H. Spiegelman, Nucl. Instrum. Methods **A234**, 455 (1985).
[18] K. S. Krane, Nucl. Phys. **A377**, 176 (1982).
[19] M. A. Lee and R. L. Bunting, Nucl. Data Sheets **48**, 187

(1985).
[20]*Table of Isotopes,* edited by C. M. Lederer and V. S. Shirley (Wiley, New York, 1978).
[21]K. S. Krane, Nucl. Instrum. Methods **98**, 205 (1972).
[22]A preliminary account of this fitting procedure was given in W. D. Brewer, P. Roman, and H. Marshak, Hyperfine Interact. **49**, 1131 (1989).
[23]These are generated by plotting Eqs. (10) and (11) as a function of δ in the $W(0)$, $W(\frac{1}{2}\pi)$ plane. It can be shown that the resulting curve is always an ellipse irregardless of the values of the coefficients F_λ, B_λ, U_λ, and Q_λ, unless $\delta=0$, when the ellipse then degenerates to a point.
[24]J. Jin, J. Takada, Y. Iwata, and Y. Yoshizawa, Nucl. Instrum. Methods **212**, 259 (1982).
[25]I. I. Gromova, Ya. Dupak, Ya. Konichek, T. I. Kratsikova, N. A. Lebedev, B. S. Neganov, V. N. Pavlov, I. Prokhazka, M. Finger, V. M. Tsupko-Sitnikov, A. F. Shus, A. Makhova, W. D. Hamilton, and R. A. Fox, Izv. Akad. Nauk SSSR, Ser. Fiz. **43**, 53 (1979) [Bull. Acad. Sci. USSR, Phys. Ser. **43**, 422 (1979)].
[26]R. A. Fox, W. D. Hamilton, and D. D. Warner, J. Phys. A **7**, 1716 (1974).
[27]A. L. Erzinkyan, V. V. Murav'eva, V. P. Parfenova, V. V. Turovtsev, and V. S. Shpinel', Zh. Eksp. Teor. Fiz. **72**, 1902 (1977) [Sov. Phys.—JETP **45**, 999 (1977)].
[28]S. Kobayashi, N. Sano, and J. Itoh, J. Phys. Soc. Jpn. **23**, 474 (1967).
[29]C. Günther, H. Ryde, and K. Krein, Nucl. Phys. **A122**, 401 (1968).
[30]S. S. Bhati, N. Singh, P. D. Bajaj, and P. N. Trehan, Aust. J. Phys. **29**, 405 (1976).
[31]P. L. Gardulski and M. L. Wiedenbeck, Phys. Rev. C **7**, 2080 (1973).
[32]K. S. Krane and R. M. Steffen, Nucl. Phys. **A164**, 439 (1971).
[33]J. M. Jaklevic, E. G. Funk, and J. W. Mihelich, Nucl. Phys. **A99**, 83 (1967).
[34]F. C. Zawislak, J. D. Rogers, and E. A. Menêses, Nucl. Phys. **A211**, 581 (1973).
[35]R. N. Oehlberg, L. L. Riedinger, A. E. Rainis, A. G. Schmidt, E. G. Funk, and J. W. Mihelich, Nucl. Phys. **A219**, 543 (1974).
[36]F. K. McGowan and W. T. Milner, Phys. Rev. C **23**, 1926 (1981).
[37]J. Lange, in *Proceedings of the International Conference on Angular Correlations in Nuclear Disintegration, Delft, 1970,* edited by H. van Krugten and B. van Nooijen (Rotterdam University Press, Rotterdam, 1971), p. 242.
[38]D. D. Warner, Phys. Rev. Lett. **47**, 1819 (1981).
[39]K. S. Krane, Phys. Rev. C **8**, 1494 (1973).